

NIKHEF/97-007

INLO-PUB-2/97

$\mathcal{O}(\alpha_s^2)$ Contributions to charm production in charged-current deep-inelastic lepton-hadron scattering

M. BUZA ¹*NIKHEF/UVA,**POB 41882, NL-1009 DB Amsterdam,**The Netherlands.*

W.L. VAN NEERVEN

*Instituut-Lorentz,**University of Leiden,**PO Box 9506, 2300 RA Leiden,**The Netherlands.*

February 1997

Abstract

The most important part of the order α_s^2 corrections to the charm component of the charged-current structure functions $F_2(x, Q^2)$ and $F_3(x, Q^2)$ have been calculated. This calculation is based on the asymptotic form of the heavy-quark coefficient functions corresponding to the higher order corrections to the W-boson-gluon fusion process. These coefficient functions which are in principle only valid for $Q^2 \gg m^2$ can be also used to estimate the order α_s^2 contributions at lower Q^2 values provided $x < 0.1$. It turns out that the above corrections are appreciable in the large Q^2 -region and they explain the discrepancy found for the structure functions between the fixed-flavour scheme (FFS) and the variable-flavour-number scheme (VFNS). These corrections also hamper the extraction of the strange-quark density from the data obtained for the charged-current and the electromagnetic-current processes.

¹supported by the Foundation for Fundamental Research on Matter (FOM)

1 Introduction

The study of charm production in deep-inelastic lepton-hadron scatterings provides us with important information about heavy-quark production mechanisms. The latter enables us to extract parton densities from the deep-inelastic data in certain kinematical regions which are difficult to explore in other hard processes. The best example is the gluon density $G(x, \mu^2)$ where μ denotes the factorization scale. It can be measured at small x in deep-inelastic electroproduction $e^\pm + N \rightarrow e^\pm + 'X'$ via the photon-gluon fusion process

$$\gamma^* + g \rightarrow c + \bar{c} \quad (1.1)$$

where $'X'$ denotes any inclusive final state. The above process dominates electroproduction of the charm quark if one assumes that the probability to find a charm quark inside the proton is zero so that the flavour-excitation process

$$\gamma^* + c \rightarrow c \quad (1.2)$$

does not occur. The reactions (1.1) and (1.2) are sometimes also referred to as extrinsic- and intrinsic-charm production. In the subsequent part of this paper we will assume that there is no charm quark in the initial state. Another parton density which can be measured via charm production is the strange-quark density $s(x, \mu^2)$. The latter shows up in the charged-current process $\nu(\bar{\nu}) + p \rightarrow l^-(l^+) + 'X'$ ($l = e, \mu$) which in lowest order is given by the flavour-excitation mechanism

$$W^+ + s \rightarrow c, \quad W^- + \bar{s} \rightarrow \bar{c}. \quad (1.3)$$

In next-to-leading order (NLO) we have the following parton subprocesses. The first one is represented by the gluon bremsstrahlung process

$$W^+ + s \rightarrow c + g, \quad W^- + \bar{s} \rightarrow \bar{c} + g \quad (1.4)$$

which includes the one-loop corrections to the Born reaction (1.3). Furthermore we have the W-boson-gluon fusion mechanism given by

$$W^+ + g \rightarrow c + \bar{s}, \quad W^- + g \rightarrow \bar{c} + s. \quad (1.5)$$

Although for $x \geq 0.1$ charm production is determined by flavour excitation it turns out that the W-boson-gluon fusion process dominates the order α_s corrections for $x < 0.1$ and constitutes a large background for reaction (1.3). This means that in the region $x < 0.1$ an accurate determination of $s(x, \mu^2)$ requires a good knowledge of $G(x, \mu^2)$. Charm production in charged-current interactions was studied in the experiments carried out by the CCFR-collaboration in [1], [2]. Besides the strange-quark density one has also determined one of the elements of the CKM (Cabibbo-Kobayashi-Moskawa) matrix, called $|V_{cd}|$, which is approximately equal to $|\sin \theta_C|$ where θ_C denotes the Cabbibo angle. However there exists an alternative way to determine the strange-quark density $s(x, \mu^2)$. Here the latter follows from the relation

$$\Delta(x, \mu^2) = \frac{5}{6} F_2^{\nu N}(x, \mu^2) - 3 F_2^{\mu N}(x, \mu^2). \quad (1.6)$$

Here $F_2^{\nu N}$ and $F_2^{\mu N}$ are the structure functions corresponding to charged-current and electromagnetic-current induced processes respectively, where N is represented by an isoscalar nuclear target. Neglecting nuclear corrections one obtains

$$F_2^{lN}(x, \mu^2) = \frac{1}{2} \left(F_2^{lp}(x, \mu^2) + F_2^{ln}(x, \mu^2) \right) \quad (1.7)$$

with $l = e^\pm, \mu^\pm, \bar{\nu}_e, \bar{\nu}_\mu$ and p and n stand for the proton and the neutron respectively. Further F_2^{lN} denotes the full structure function where besides charm-quark production also the other light-parton (u,d,s,g) subprocesses are involved. If the structure functions appearing on the right-hand side of (1.6) are computed on the Born level we obtain in a three-flavour scheme

$$\Delta(x, \mu^2) = x s(x, \mu^2). \quad (1.8)$$

In the case of a four-flavour scheme where now also the charm quark is represented by a parton density Eq. (1.6) becomes

$$\Delta(x, \mu^2) = x s(x, \mu^2) - x c(x, \mu^2). \quad (1.9)$$

The three- and four-flavour scheme are in the literature very often referred to as fixed-flavour scheme (FFS) and variable-flavour-number scheme (VFNS) respectively. The structure functions $F_2^{\nu N}$ and $F_2^{\mu N}$ have been measured by the CCFR collaboration [3], [4] and the NMC-collaboration [5]. If one takes the data from [3], [5] then the result obtained for $s(x, \mu^2)$ is quite close to the one measured in charm production [1], [2] (see also the discussion in [6]). However there exists a discrepancy between the data of [3] and [4] which is not clarified yet. If we adopt the three-flavour scheme for the subsequent part of our paper the identity in (1.8) only holds if the charm-quark mass is zero and the QCD corrections are neglected. However as we will see later on these corrections will considerably alter Eq. (1.8) in particular in the small x -region. This is mainly due to the W-boson-gluon fusion process in (1.5) and its higher order QCD corrections. The corrections due to the mass of the charm quark become smaller when the virtuality of the W-boson denoted by Q^2 will become very large. The order α_s corrections given by the reactions (1.4), (1.5) were calculated in [7] (see also [6], [8]). The dependence on the mass of the charm quark was studied in [9] and a comparison between the FFS [10] and VFNS [11] was made in [12], [13]. In the latter references the dependence of the QCD corrected structure functions on the factorization scale was studied too. One of the main conclusions of these investigations is that the QCD corrections for $x \geq 0.1$ are small whereas for $x < 0.1$ the bulk of the corrections is constituted by the W-boson-gluon fusion process (1.5). These corrections become even larger when Q^2 increases. In particular at HERA [14], [15], [16] where $200 < Q^2 < 10^4$ (GeV/c)², the size of the contribution of the latter process is responsible for the discrepancy between the FFS and VFNS in describing the charm component of the structure functions denoted by $F_{k,c}$ ($k = 2, 3$) as discussed in [13]. Therefore we will concentrate ourselves in this paper on the calculation of the order α_s^2 contributions to $F_{k,c}$ which are due to the order α_s corrections to the W-boson-gluon fusion process in (1.5). This also includes the contributions from other heavy-quark subprocesses initiated by the light quarks u, d and s. Unfortunately for some of them we only have the asymptotic expressions of the heavy-quark coefficient functions which are valid for $Q^2 \gg m^2$ where m stands for the heavy-quark mass. This implies that strictly speaking they are only applicable to the HERA experiments where the characteristic values for Q^2 are very large. However as is shown for the electromagnetic-current process [17]-[20], where the exact order α_s corrections to the photon-gluon fusion process are known

[21], the asymptotic heavy-quark coefficient functions can be used for much lower Q^2 values measured at fixed-target experiments. If Q^2 is an order of magnitude larger than m^2 one gets a reasonable agreement within 10% between the predictions obtained from the exact and asymptotic heavy-quark coefficient functions (see [18]-[20]).

Our paper will be organized as follows. In Section 2 we present the formulae for the charged-current deep-inelastic structure functions expressed in convolutions of the parton densities and the coefficient functions. Further we construct the asymptotic form of the order α_s^2 contributions to the heavy-quark coefficient functions. In Section 3 we discuss our results and show the effect of the latter on the charm component of the charged-current structure functions. We also show how the extraction of the strange density from relation (1.6) is influenced by the above corrections. The derivation of the asymptotic heavy-quark coefficient functions will be presented in Appendix A.

2 $\mathcal{O}(\alpha_s^2)$ contributions to heavy-flavour coefficient functions in charged-current interactions

In this section we will present the asymptotic forms of the heavy-quark coefficient functions up to order α_s^2 which contribute to the structure functions $F_2(x, Q^2)$ and $F_3(x, Q^2)$ measured in charged-current deep-inelastic lepton-hadron scattering. Although these coefficient functions are only valid at $Q^2 \gg m^2$, characteristic of the values of Q^2 observed at HERA, they can be also used to make a reasonable estimate of the charm component of the structure functions measured in fixed-target experiments where Q^2 is much smaller. Here and in the next section we will compute all structure functions in the so called fixed-flavour scheme (FFS). In the case of the charm production this means that the constituents of the hadron are only given by the gluon and the three light flavours u,d,s which are described by parton densities. The charm quark only appears in the final state of the parton subprocesses and its contribution to the structure functions is described by the heavy-quark coefficient functions. As is shown in [20] the FFS is suitable to describe the charm component to the structure functions at small Q^2 -values. However at large Q^2 where the large logarithms of the type $\ln^i(Q^2/m^2) \ln^j(\mu^2/m^2)$ dominate the heavy-quark coefficient functions this description is not adequate anymore. In this regime it is much more useful to adopt the variable-flavour-number scheme (VFNS) where now also the charm-quark contribution is described by a parton density. This parton density represents the resummation of the large logarithms above in all orders of perturbation theory. We will comment on the VFNS approach in the case of charm production at HERA collider in the next section. In the FFS (here three-flavour scheme) the light-parton contribution to the structure functions measured in the process $\nu_l + p \rightarrow l + X'$ ($l = e, \mu$) is given by

$$\begin{aligned}
F_k^{W^+p}(x, Q^2) &\equiv F_k^{\nu p}(x, Q^2) = \\
&a_k(x) \int_x^1 \frac{dz}{z} \left[\Sigma_3\left(\frac{x}{z}, \mu^2\right) \tilde{C}_{k,q}^{\text{PS}}\left(z, \frac{Q^2}{\mu^2}\right) + G\left(\frac{x}{z}, \mu^2\right) \tilde{C}_{k,g}^{\text{S}}\left(z, \frac{Q^2}{\mu^2}\right) \right. \\
&\quad \left. + \left\{ b_{k,\bar{u}} \bar{u}\left(\frac{x}{z}, \mu^2\right) + b_{k,d} \cos^2(\theta_C) d\left(\frac{x}{z}, \mu^2\right) \right\} \right]
\end{aligned}$$

$$+b_{k,s} \sin^2(\theta_C) s \left(\frac{x}{z}, \mu^2 \right) \left\} \mathcal{C}_{k,q}^{\text{NS}} \left(z, \frac{Q^2}{\mu^2} \right) \right] \quad (2.1)$$

with

$$a_2(x) = 2x, \quad a_3(x) = 2 \quad (2.2)$$

and for $i = u, d, s$; $\bar{i} = \bar{u}, \bar{d}, \bar{s}$

$$b_{2,i} = b_{3,i} = 1, \quad b_{2,\bar{i}} = -b_{3,\bar{i}} = 1. \quad (2.3)$$

Here $G(z, \mu^2)$ denotes the gluon density and the singlet combination of parton densities in the three-flavour scheme is given by

$$\begin{aligned} \Sigma_3(z, \mu^2) = & u(z, \mu^2) + \bar{u}(z, \mu^2) + d(z, \mu^2) + \bar{d}(z, \mu^2) \\ & + s(z, \mu^2) + \bar{s}(z, \mu^2). \end{aligned} \quad (2.4)$$

Like the parton densities the coefficient functions $\mathcal{C}_{k,i}$ ($k = 2, 3$; $i = q, g$) can be distinguished into a singlet and non-singlet part indicated by the superscripts S and NS respectively. In (2.1) we have split the singlet coefficient function $\mathcal{C}_{k,q}^{\text{S}}$ in the following way

$$\mathcal{C}_{k,q}^{\text{S}} = \mathcal{C}_{k,q}^{\text{NS}} + \mathcal{C}_{k,q}^{\text{PS}}. \quad (2.5)$$

The purely-singlet part of the coefficient function indicated by PS originates from quark subprocesses where the projection on the non-singlet channel yields zero, so that only singlet contributions remain. They are characterized by those Feynman graphs in which only gluons are exchanged in the t-channel. Such graphs show up for the first time in order α_s^2 . Furthermore because of charge conjugation invariance of the strong interactions one has the property

$$\tilde{\mathcal{C}}_{3,q}^{\text{PS}} = 0, \quad \tilde{\mathcal{C}}_{3,g}^{\text{S}} = 0, \quad (2.6)$$

so that F_3 is determined by the non-singlet combination of parton densities and $\mathcal{C}_{3,q}^{\text{NS}}$ only. In the case of F_2 we have extracted the overall dependence of the coefficient functions $\mathcal{C}_{2,q}^{\text{PS}}$ and $\mathcal{C}_{2,g}^{\text{S}}$ on the number of light flavours n_f so that we will denote them by $\tilde{\mathcal{C}}_{2,q}^{\text{PS}}$ and $\tilde{\mathcal{C}}_{2,g}^{\text{S}}$ respectively. Finally, in the three-flavour scheme, the structure functions depend on the Cabbibo angle θ_C only.

The charm contribution to the structure functions $F_k^{\nu p}$ ($k = 2, 3$) can be written as

$$\begin{aligned}
F_{k,c}^{W^+p}(x, Q^2, m^2) &\equiv F_{k,c}^{\nu p}(x, Q^2, m^2) = \\
&a_k(x) \int_x^{z_{th}} \frac{dz}{z} \left[\Sigma_3\left(\frac{x}{z}, \mu^2\right) L_{k,q}^{W,PS}\left(z, \frac{Q^2}{m^2}, \frac{m^2}{\mu^2}\right) + G\left(\frac{x}{z}, \mu^2\right) L_{k,g}^{W,S}\left(z, \frac{Q^2}{m^2}, \frac{m^2}{\mu^2}\right) \right. \\
&+ \left\{ b_{k,\bar{u}} \bar{u}\left(\frac{x}{z}, \mu^2\right) + b_{k,d} \cos^2(\theta_C) d\left(\frac{x}{z}, \mu^2\right) + b_{k,s} \sin^2(\theta_C) s\left(\frac{x}{z}, \mu^2\right) \right\} \\
&\times L_{k,q}^{W,NS}\left(z, \frac{Q^2}{m^2}, \frac{m^2}{\mu^2}\right) \Big] + a_k(x) \int_x^{z'_{th}} \frac{dz}{z} \left[\Sigma_3\left(\frac{x}{z}, \mu^2\right) H_{k,q}^{W,PS}\left(z, \frac{Q^2}{m^2}, \frac{m^2}{\mu^2}\right) \right. \\
&+ G\left(\frac{x}{z}, \mu^2\right) H_{k,g}^{W,S}\left(z, \frac{Q^2}{m^2}, \frac{m^2}{\mu^2}\right) + \left\{ b_{k,d} \sin^2(\theta_C) d\left(\frac{x}{z}, \mu^2\right) \right. \\
&+ \left. \left. b_{k,s} \cos^2(\theta_C) s\left(\frac{x}{z}, \mu^2\right) \right\} H_{k,q}^{W,NS}\left(z, \frac{Q^2}{m^2}, \frac{m^2}{\mu^2}\right) \Big] \quad (2.7)
\end{aligned}$$

with

$$z_{th} = \frac{Q^2}{Q^2 + 4m^2}, \quad z'_{th} = \frac{Q^2}{Q^2 + m^2}. \quad (2.8)$$

The above upper boundaries of the integrals in (2.7) follow from the threshold conditions. In the first part of Eq. (2.7) the heavy-quark coefficient functions $L_{k,i}^W$ originate from parton subprocesses with a heavy quark and a heavy anti-quark in the final state. Here the W-boson is attached to the light quarks u,d,s only. Hence the partonic centre of mass energy squared \hat{s} has to satisfy the condition $\hat{s} \geq 4m^2$ with $\hat{s} = Q^2(1-z)/z$. In the second part of (2.7) the heavy-quark coefficient functions $H_{k,i}^W$ originate from the parton subprocesses where either the heavy quark or the heavy anti-quark appears in the final state which is accompanied by a light (anti-) quark. Furthermore the W-boson also couples to the heavy (anti-) quark. Therefore $\hat{s} \geq m^2$. Notice that in (2.7) we have limited ourselves to those parton subprocesses which have no more than two heavy (anti-) quarks in the final state. The notation in (2.7) is the same as given for the light-parton contributions to the structure functions listed below (2.1). Because of charge conjugation invariance of the strong interactions the $L_{k,i}^W$ satisfy similar relations as quoted in (2.6) i.e.

$$L_{3,q}^{W,PS} = 0, \quad L_{3,g}^{W,S} = 0. \quad (2.9)$$

The structure functions $F_k^{\bar{\nu}p}$ and $F_{k,c}^{\bar{\nu}p}$ which show up in the anti-neutrino reaction $\bar{\nu}_l + p \rightarrow \bar{l} + X'$ can be derived from Eqs. (2.1) and (2.7) by the replacements $u \leftrightarrow \bar{u}$, $d \leftrightarrow \bar{d}$, $s \leftrightarrow \bar{s}$. Moreover in the case of $F_{3,c}^{\bar{\nu}p}$ the heavy-quark coefficient functions $H_{3,q}^{W,PS}$ and $H_{3,g}^{W,S}$ get a relative minus sign with respect to the ones showing up in $F_{3,c}^{\nu p}$ (2.7).

In the case of an isoscalar target one also has to compute the structure functions for the neutron given by $F_k^{\nu n}$, $F_k^{\bar{\nu}n}$, $F_{k,c}^{\nu n}$, $F_{k,c}^{\bar{\nu}n}$. The latter can be derived from the proton structure functions by the replacements $u \leftrightarrow d$ and $\bar{u} \leftrightarrow \bar{d}$.

In the next section we want to compute the structure functions in (2.1) and (2.7) up to next-to-leading order (NLO). Moreover we want to include the order α_s^2 contributions to the heavy-quark coefficient functions $L_{k,q}^{W,NS}$, $H_{k,q}^{W,PS}$ and $H_{k,g}^{W,S}$ appearing in $F_{k,c}^{\nu p}$ (2.7). Notice that up to order α_s^2 the coefficient functions $L_{2,q}^{W,PS}$ and $L_{2,g}^{W,S}$ do not contribute because the corresponding parton subprocesses are of the order α_s^4 and α_s^3 respectively. For $L_{3,q}^{W,PS}$ and $L_{3,g}^{W,S}$ see (2.9). Furthermore we do not include the order α_s^2 contributions to $H_{k,q}^{W,NS}$. The latter coefficient function is determined by the higher order QCD corrections to the flavour-excitation process (1.3). In order α_s it turns out that these corrections are much smaller than those originating from the W-boson-gluon fusion process (1.5) leading to the coefficient function $H_{k,g}^{W,S}$. Hence we expect that beyond order α_s the radiative corrections are dominated by the W-boson-gluon fusion mechanism which is also indirectly present in the parton subprocess contributing to $H_{k,q}^{W,PS}$.

For the computation of $F_k^{\nu p}$, $F_k^{\bar{\nu}p}$ (2.1) one needs the next-to-leading-log (NLL) parton densities and the light-parton coefficient functions $\mathcal{C}_{k,i}$ ($k = 2, 3; i = q, g$) corrected up to order α_s . Notice that $\tilde{\mathcal{C}}_{2,q}^{PS}$ vanishes up to this order. The representation in the \overline{MS} -scheme can be found in Appendix I of [22]. For the calculation of $F_{k,c}^{\nu p}$, $F_{k,c}^{\bar{\nu}p}$ the heavy-quark coefficient functions $H_{k,q}^{W,NS}$ and $H_{k,g}^{W,S}$ have been computed in [7] up to order α_s (see also [6], [8]). The latter are represented in the \overline{MS} -scheme in Appendix A of [6]. In this paper we want to compute the order α_s^2 contributions to $L_{k,q}^{W,NS}$, $H_{k,q}^{W,PS}$ and $H_{k,g}^{W,S}$. The coefficient function $L_{k,q}^{W,NS}$ is given by the Compton reaction

$$W + q(\bar{q}) \rightarrow q'(\bar{q}') + c + \bar{c} \quad (2.10)$$

where the heavy-quark pair originates from gluon splitting and the gluon is radiated off the light quarks q and q' ($q, q' = u, d, s$). The reaction above also includes the two-loop vertex correction to the subprocess $W + q(\bar{q}) \rightarrow q'(\bar{q}')$ containing the charm-loop contribution to the gluon self-energy. This we do in order to improve the large Q^2 behaviour of the coefficient function. Without this vertex correction $L_{k,q}^{W,NS} \sim \ln^3(Q^2/m^2)$ whereas it behaves like $\ln^2(Q^2/m^2)$ if this correction has been included. The coefficient function $H_{k,q}^{W,PS}$ is computed from the Bethe-Heitler process given by the reaction

$$W + q(\bar{q}) \rightarrow q(\bar{q}) + c(\bar{c}) + \bar{q}'(q') \quad (2.11)$$

with $q = u, d, s$ and $q' = d, s$. Like reaction (2.10) process (2.11) shows up for the first time if the QCD corrections are calculated up to order α_s^2 . Contrary to (2.10), where the W-boson is only attached to the light quarks q and q' , the vector boson in reaction (2.11) is now coupled to the charm quark and the light quark q' . Finally we have the W-boson-gluon fusion mechanism which contributes to $H_{k,g}^{W,S}$. In order α_s (lowest order) this production mechanism is given by the process (see also (1.5))

$$W + g \rightarrow c(\bar{c}) + \bar{q}'(q') \quad (2.12)$$

with $q' = d, s$. In NLO we have to include all virtual corrections to reaction (2.12) and to add the contributions due to the gluon bremsstrahlung process

$$W + g \rightarrow c(\bar{c}) + \bar{q}'(q') + g. \quad (2.13)$$

Contrary to $L_{k,q}^{W,NS}$ for which the exact order α_s^2 expressions exist, see [17] ($k = 2$) and [18] ($k = 3$) we do not have the exact form of $H_{k,q}^{W,PS}$ and $H_{k,g}^{W,S}$ in the same order. This is in contrast to the heavy-flavour electroproduction where the deep-inelastic process only proceeds via the exchange of a virtual photon. In this case the exact order α_s^2 contributions to the heavy-quark

coefficients $H_{2,q}^{\gamma,\text{PS}}$ and $H_{2,q}^{\gamma,\text{S}}$ are known and they can be found in [17]. For the charged-current process the calculation of these coefficient functions is still more difficult than the ones for the electromagnetic-current reaction as given above. This can be attributed to the mass of the light quarks q' in (2.11)-(2.13) which is usually put to be equal to zero. Therefore the power of the collinear singularities, occurring in the higher order radiative corrections to the charged-current reaction, is much higher than the one appearing in the electromagnetic-current process where also q' stands for the charm quark. This in particular will complicate the calculation of the many particle phase space integrals. The latter are even more complicated than those encountered in parton subprocesses where all masses of the particles in the final state are equal to zero. These type of phase space integrals have been calculated in [23]. However these complications can be avoided if one is only interested in the asymptotic form of the heavy-quark coefficient functions given for $Q^2 \gg m^2$. This form can be derived using the renormalization group and mass-factorization techniques. These methods have been applied to obtain the heavy-quark coefficient functions in the limit $Q^2 \gg m^2$ for unpolarized [17] and polarized [18] electromagnetic-current deep-inelastic lepton-hadron scattering processes. Here in the FFS the light parton contribution to the structure function $F_2^{lp}(x, Q^2)$ ($l = e, \mu$) is given by

$$\begin{aligned}
F_2^{\gamma p}(x, Q^2) \equiv F_2^{lp}(x, Q^2) = & x \int_x^1 \frac{dz}{z} \left[\frac{2}{3} \left\{ \Sigma_3 \left(\frac{x}{z}, \mu^2 \right) \tilde{\mathcal{C}}_{2,q}^{\text{PS}}(z, \mu^2) \right. \right. \\
& + G \left(\frac{x}{z}, \mu^2 \right) \tilde{\mathcal{C}}_{2,g}^{\text{S}}(z, \mu^2) \left. \right\} + \left\{ \frac{4}{9} \left[u \left(\frac{x}{z}, \mu^2 \right) + \bar{u} \left(\frac{x}{z}, \mu^2 \right) \right] \right. \\
& \left. \left. + \frac{1}{9} \left[d \left(\frac{x}{z}, \mu^2 \right) + \bar{d} \left(\frac{x}{z}, \mu^2 \right) + s \left(\frac{x}{z}, \mu^2 \right) + \bar{s} \left(\frac{x}{z}, \mu^2 \right) \right] \right\} \mathcal{C}_{2,q}^{\text{NS}}(z, \mu^2) \right] \quad (2.14)
\end{aligned}$$

and the charm component reads

$$\begin{aligned}
F_{2,c}^{\gamma p}(x, Q^2, m^2) \equiv F_{2,c}^{lp}(x, Q^2, m^2) = & x \int_x^{z_{th}} \frac{dz}{z} \left[\frac{2}{3} \left\{ \Sigma_3 \left(\frac{x}{z}, \mu^2 \right) \right. \right. \\
& \times L_{2,q}^{\gamma,\text{PS}} \left(z, \frac{Q^2}{m^2}, \frac{m^2}{\mu^2} \right) + G \left(\frac{x}{z}, \mu^2 \right) L_{2,g}^{\gamma,\text{S}} \left(z, \frac{Q^2}{m^2}, \frac{m^2}{\mu^2} \right) \left. \right\} + \left\{ \frac{4}{9} \left[u \left(\frac{x}{z}, \mu^2 \right) \right. \right. \\
& \left. \left. + \bar{u} \left(\frac{x}{z}, \mu^2 \right) \right] + \frac{1}{9} \left[d \left(\frac{x}{z}, \mu^2 \right) + \bar{d} \left(\frac{x}{z}, \mu^2 \right) + s \left(\frac{x}{z}, \mu^2 \right) + \bar{s} \left(\frac{x}{z}, \mu^2 \right) \right] \right\}
\end{aligned}$$

$$\begin{aligned}
& \times L_{2,q}^{\gamma,\text{NS}}\left(z, \frac{Q^2}{m^2}, \frac{m^2}{\mu^2}\right) \Big] + \frac{4}{9}x \int_x^{z_{th}} \frac{dz}{z} \left[\Sigma_3\left(\frac{x}{z}, \mu^2\right) H_{2,q}^{\gamma,\text{PS}}\left(z, \frac{Q^2}{m^2}, \frac{m^2}{\mu^2}\right) \right. \\
& \left. + G\left(\frac{x}{z}, \mu^2\right) H_{2,g}^{\gamma,\text{S}}\left(z, \frac{Q^2}{m^2}, \frac{m^2}{\mu^2}\right) \right]. \tag{2.15}
\end{aligned}$$

The notations above are the same as those given for the charged-current structure functions in (2.1) and (2.7). Notice that the light-parton coefficient functions $\mathcal{C}_{k,i}$ are the same in both reactions which means that they do not depend on the probe W or γ . This does not hold for the heavy-quark coefficient functions. The most important result of these calculations is that the $F_{2,c}^{lp}(x, Q^2)$ does not change when the exact heavy-quark coefficient functions are replaced by their asymptotic expressions provided $Q^2 > Q_{min}^2$. In the case of charm production $Q_{min}^2 = 20 \text{ (GeV/c)}^2$ for $x < 0.1$. Furthermore it turns out that the value obtained for Q_{min}^2 is not altered while going from the LO to the NLO approximation. If we now assume that the same property also holds for the charged-current structure functions $F_k^{\nu p}(x, Q^2)$, $F_k^{\bar{\nu} p}(x, Q^2)$ then the asymptotic forms of $H_{k,i}^W$ can be used to make fairly good predictions of the order α_s^2 contributions. These predictions will become very accurate for experiments carried out at HERA since the Q^2 -values are very large and the x -values are reasonable small i.e. $200 < Q^2 < 10^4 \text{ (GeV/c)}^2$ and $0.006 < x < 0.5$. Even for fixed-target experiments where the characteristic Q^2 -values are much smaller one can make reliable predictions unless one enters the threshold region where Q^2 is too small ($Q^2 < 20 \text{ (GeV/c)}^2$) and/or x is too large ($x > 0.1$).

The asymptotic heavy-quark coefficient functions $H_{k,i}^W$ for the charged-current process are derived in Appendix A. It appears that they can be expressed into the asymptotic heavy-quark coefficient functions $H_{k,i}^\gamma$ in (2.15) computed for the electromagnetic-current process (see Appendix D of [17]). Let us first first expand these coefficient functions in a power series like

$$H_{k,i}^V = \sum_{l=1}^{\infty} \left(\frac{\alpha_s}{4\pi} \right)^l H_{k,i}^{V,(l)} \tag{2.16}$$

with $V = \gamma, W$; $k = 2, 3$ and $i = q, g$. From Appendix A it follows that the coefficients $H_{k,i}^{V,(l)}$ up to order α_s^2 in the limit $Q^2 \gg m^2$ are related to each other as follows

$$H_{k,g}^{W,S,(1)}\left(z, \frac{Q^2}{m^2}, \frac{m^2}{\mu^2}\right) = \frac{1}{2}H_{2,g}^{\gamma,S,(1)}\left(z, \frac{Q^2}{m^2}, \frac{m^2}{\mu^2}\right) + \frac{1}{2}\epsilon_k \tilde{C}_{2,g}^{S,(1)}\left(z, \frac{Q^2}{\mu^2}\right), \quad (2.17)$$

$$\begin{aligned} H_{k,g}^{W,S,(2)}\left(z, \frac{Q^2}{m^2}, \frac{m^2}{\mu^2}\right) &= \frac{1}{2}H_{2,g}^{\gamma,S,(2)}\left(z, \frac{Q^2}{m^2}, \frac{m^2}{\mu^2}\right) + \frac{1}{2}\epsilon_k \tilde{C}_{2,g}^{S,(2)}\left(z, \frac{Q^2}{\mu^2}\right) \\ &+ \frac{1}{2} \int_z^1 \frac{dy}{y} A_{cg}^{S,(1)}\left(\frac{z}{y}, \frac{m^2}{\mu^2}\right) \left\{ \mathcal{C}_{k,q}^{S,(1)}\left(z, \frac{Q^2}{\mu^2}\right) - \mathcal{C}_{2,q}^{S,(1)}\left(z, \frac{Q^2}{\mu^2}\right) \right\}, \end{aligned} \quad (2.18)$$

$$H_{k,q}^{W,PS,(2)}\left(z, \frac{Q^2}{m^2}, \frac{m^2}{\mu^2}\right) = \frac{1}{2}H_{2,q}^{\gamma,PS,(2)}\left(z, \frac{Q^2}{m^2}, \frac{m^2}{\mu^2}\right) + \frac{1}{2}\epsilon_k \tilde{C}_{2,q}^{PS,(2)}\left(z, \frac{Q^2}{\mu^2}\right) \quad (2.19)$$

with

$$\epsilon_2 = 1, \quad \epsilon_3 = -1 \quad (2.20)$$

where $H_{2,i}^{\gamma,(l)}$ ($i = q, g$) can be found in Appendix D of [17]. Further $A_{cg}^{S,(1)}$ stands for the one-loop heavy-quark operator matrix element defined in (A.6) and $\mathcal{C}_{k,i}$ ($k = 2, 3; i = q, g$) denote the light-parton coefficient functions which are presented up to order α_s^2 in Appendix B of [23]. Here we want to emphasize that relations (2.17)-(2.19) only hold in the asymptotic limit $Q^2 \gg m^2$. Further they are presented in the $\overline{\text{MS}}$ -scheme. One can check the validity of (2.17) using the exact order α_s contributions to the coefficient functions $H_{k,g}^W$ and $H_{2,g}^\gamma$ computed in [7]. Finally notice that the second order coefficient functions $\mathcal{C}_{k,i}^{(2)}$ require the knowledge of the three-loop DGLAP splitting functions in order to make a complete next-to-next-to-leading order (NNLO) analysis of $F_{k,c}^{\nu p}$ in (2.7). However these splitting functions are not known yet so that one cannot obtain the parton densities in the next-to-next-to-leading log (NNLL) approximation. Hence the order α_s^2 contributions to the structure functions $F_{k,c}^{\nu p}$ due to the expressions in (2.18), (2.19) have to be considered as an estimate of the exact QCD corrections beyond NLO. However in practice it turns out that the contributions due to the coefficient functions are much more important than those coming from the higher order DGLAP splitting functions provided both are represented in the $\overline{\text{MS}}$ -scheme (see [24]).

3 $\mathcal{O}(\alpha_s^2)$ contributions to the charged-current process due to charm production

In this section we will discuss the QCD corrections to the charged-current structure functions $F_{k,c}(x, Q^2, m^2)$ ($k = 2, 3$) measured at fixed isoscalar target experiments : $(\nu_\mu(\bar{\nu}_\mu) + N \rightarrow \mu^-(\mu^+) + X')$ [1]-[4] and the collider experiments at HERA : $(e^-(e^+) + p \rightarrow \nu_e(\bar{\nu}_e) + X')$ [14]-[16]. The kinematical ranges in which the fixed-target experiments are carried out are given by $0.01 < x < 1$ and $2 < Q^2 < 100$ (GeV/c)². For HERA they become $0.006 < x < 0.5$ and $200 < Q^2 < 10^4$ (GeV/c)². In particular we are interested in the order α_s^2 contributions originating from the heavy-quark coefficient functions $L_{k,q}^{W,NS,(2)}$ (exact) and $H_{k,q}^{W,PS,(2)}$, $H_{k,g}^{W,S,(2)}$ (asymptotic) presented in the previous section. Since we are dealing with approximations to the above contributions only we have to determine the kinematical range in which they are valid. First we have to investigate for which x - and Q^2 -values the order α_s corrections coming from $H_{k,g}^{W,S,(1)}$ (W- boson-gluon fusion process) dominate those which are due to $H_{k,q}^{W,NS,(1)}$ (flavour-excitation process). Then we have to determine Q_{min}^2 so that for $Q^2 > Q_{min}^2$ the results obtained from the asymptotic and exact expressions of the heavy-quark coefficient function $H_{k,g}^{W,S,(1)}$ coincide. Because of the observations made in [18]-[20] for the one-photon exchange process we expect that the same values of Q_{min}^2 also holds for the order α_s^2 contributions to the charged-current interactions given by $H_{k,q}^{W,PS,(2)}$, $H_{k,g}^{W,S,(2)}$.

In our plots we will use the notations that $F_{k,c}^{(l)}$ ($l = 0, 1, 2$) receive contributions from the coefficients corrected up to order α_s^l . This implies that for $F_{k,c}^{(0)}$ (Born-approximation or LO) we have to adopt the leading log (LL) parton densities and the running coupling constant. In the case of $F_{k,c}^{(1)}$ (NLO) we have to choose the next-to-leading log (NLL) parton densities and the running coupling constant. This will be also done for $F_{k,c}^{(2)}$ where we only have included the order α_s^2 contributions due to the heavy-quark coefficient functions $L_{k,q}^{W,NS,(2)}$, $H_{k,q}^{W,PS,(2)}$ and $H_{k,g}^{W,S,(2)}$. All parton densities, coefficient functions and the running coupling constant are presented in the $\overline{\text{MS}}$ -scheme. Further we choose the factorization scale equal to the renormalization scale and set $\mu^2 = Q^2$. For other scales and the scale dependence of $F_{k,c}$ see [12], [13]. The structure functions in (2.7) are presented in the fixed-flavour

scheme (FFS) where the number of light flavours is chosen to be $n_f = 3$. Since the parton density set GRV94 [25] is the only one which is consistently determined in the FFS we will adopt this in our paper. In LO and NLO the QCD scale Λ_{n_f} , which has to be substituted in the running coupling constant, is given by $\Lambda_3^{(\text{LO})} = 248 \text{ MeV}$ and $\Lambda_3^{(\text{NLO})} = 232 \text{ MeV}$ respectively. The remaining input parameters are the charm-quark mass and the Cabibbo angle which are chosen to be $m = 1.5 \text{ (GeV/c)}$ and $|\sin \theta_C| = 0.221$ [26]. For the dependence of $F_{k,c}$ on m see [9].

In order to determine the kinematical range in which the approximations are valid we will first plot the quantities $F_{k,c}^q$ and $F_{k,c}^g$ which receive the order α_s contributions from $H_{k,q}^{W,\text{NS},(1)}$ and $H_{k,g}^{W,\text{S},(1)}$ respectively. In Fig. 1 we have presented $F_{2,c}^q$, $F_{2,c}^g$ for an isoscalar target in neutrino reactions at $Q^2 = 10, 100 \text{ (GeV/c)}^2$. Here one observes that the W-boson-gluon fusion process ($F_{2,c}^g$) dominates the flavour-excitation process ($F_{2,c}^q$) when $x < 0.07$ ($Q^2 = 10 \text{ (GeV/c)}^2$). At larger Q^2 i.e. ($Q^2 = 100 \text{ (GeV/c)}^2$) x increases and the latter becomes equal to $x = 0.2$. The same plots are given for $F_{3,c}^q$ and $F_{3,c}^g$ in Fig. 2. It turns out that for $F_{3,c}$ the x -values, below which $F_{3,c}^g$ dominates $F_{3,c}^q$, are larger than the ones obtained for $F_{2,c}$. In Fig. 2 they become $x < 0.3$ for both $Q^2 = 10 \text{ (GeV/c)}^2$ and $Q^2 = 100 \text{ (GeV/c)}^2$. From the above we conclude that already at rather low Q^2 -values the W-boson-gluon fusion mechanism completely dominates the order α_s corrections to $F_{2,c}$ provided $x < 0.1$. This also holds for $F_{3,c}$ at even larger x -values i.e. $x < 0.3$.

Now we have to determine at which value of Q^2 , denoted by Q_{min}^2 , the exact heavy-quark coefficient function $H_{k,g}^{W,\text{S},(1)}$ can be replaced by its asymptotic expression without altering the structure functions $F_{k,c}$. For that purpose we will study the quantity

$$R_{k,c}(x, Q^2, m^2) = \frac{F_{k,c}^{g,asymp}(x, Q^2, m^2)}{F_{k,c}^{g,exact}(x, Q^2, m^2)} \quad (3.1)$$

where the numerator and the denominator are computed using the asymptotic and the exact expressions for $H_{k,g}^{W,\text{S},(1)}$ respectively. Further we focus our attention on the range $0.006 < x < 0.1$ which is explored by the fixed-target experiments and the HERA collider. The range $0.1 \geq x < 1$ falls beyond our scope because here the W-boson-gluon fusion process is not dominant any-

more. In Fig. 3 we have plotted $R_{2,c}$ in the range $10 < Q^2 < 10^4$ (GeV/c)² for $x = 0.1, 0.01, 10^{-3}, 10^{-4}$. The same is done for $R_{3,c}$ in Fig. 4. Fig. 3 reveals that for $x = 0.1$, $R_{2,c} > 0.9$ when $Q^2 > Q_{min}^2 = 50$ (GeV/c)². At decreasing x the value of Q_{min}^2 will become less so that for $x = 10^{-4}$ one obtains $Q_{min}^2 = 20$ (GeV/c)². A similar behaviour is shown by Fig. 4. Here we observe that for $x = 0.1$, $R_{3,c} > 0.9$ when $Q_{min}^2 = 85$ (GeV/c)². Also in this case Q_{min}^2 decreases if x gets lower. For instance for $x = 10^{-4}$ we get $Q_{min}^2 = 50$ (GeV/c)². From the above one cannot conclude that the replacement of the exact by the asymptotic coefficient functions works better for $F_{2,c}$ than for $F_{3,c}$. This becomes clear when Fig. 5 is compared with Fig. 6 where now $R_{k,c}$ (3.1) ($k = 2, 3$) is plotted as a function of x for $Q^2 = 10, 20, 50, 100$ (GeV/c)². If we choose $Q^2 = 10$ (GeV/c)² then in the range $0.01 < x < 0.1$ we observe that $0.6 > R_{3,c} > 0.5$ (Fig. 6). However the behaviour of $R_{2,c}$ is terrible. In the range $0.01 < x < 0.05$ we find $0.7 > R_{2,c} > 0.1$. For $x > 0.05$, $R_{2,c}$ becomes even negative and for very large x it switches sign again. This behaviour of the coefficient functions originates from mass factorization of the original partonic cross sections which destroys the positive definiteness of the latter quantities. Further we also studied the behaviour of $F_{k,c}^q$, $F_{k,c}^g$ and $R_{k,c}$ for antineutrino isoscalar reactions but the results are the same as found above. Summarizing our findings we can state that for $x < 0.1$ and $Q^2 > Q_{min}^2 = 50$ (GeV/c)² the approximation to the structure functions, given by the replacement of the exact by the asymptotic heavy-quark coefficient functions, works quite well. One can also choose smaller values for Q_{min}^2 . However in this case the approximation will still work for $F_{3,c}$ but it becomes bad for $F_{2,c}$ unless one chooses smaller values for x . For example for $Q_{min}^2 = 20$ (GeV/c)² one has to take $x < 0.08$. From now on we will assume that the same Q_{min}^2 and x also hold for the order α_s^2 contributions to the heavy-quark coefficient functions $H_{k,q}^{W,PS}$, $H_{k,g}^{W,S}$. This assumption is based on our findings in [18]-[20] for the electromagnetic-current process where the above contributions are exactly known up to order α_s^2 .

In the next figures we show $F_{2,c}^{(l)}$ ($l = 0, 1, 2$) for the neutrino isoscalar target reaction. Here we have plotted $F_{2,c}^{(0)}$ (exact), $F_{2,c}^{(1)}$ (exact) and $F_{2,c}^{(2)}$ (approximate) for $Q^2 = 10$ (GeV/c)² (Fig. 7) and $Q^2 = 100$ (GeV/c)² (Fig. 8). Fig. 7 reveals that the order α_s^2 contributions, which are positive, become very small. However here one has to bear in mind that for $x \geq 0.03$ and $Q_{min}^2 = 10$ (GeV/c)² the estimate of this contribution is not very reliable

in view of what we found in Fig. 5. At $Q^2 = 100 \text{ (GeV/c)}^2$ (Fig. 8), where the approximation is very accurate, the order α_s^2 corrections are larger and at $x = 0.01$ they amount to 5% of $F_{2,c}^{(1)}$ which is still quite small. These corrections in the case of $F_{3,c}$ (see Figs. 9,10) become much larger than the ones observed for $F_{2,c}$. Furthermore in the light of the discussion above for $R_{3,c}$ (Fig. 6) they are more reliable even for $Q^2 = 10 \text{ (GeV/c)}^2$ (Fig. 9). Like in the case of $F_{2,c}$ the largest corrections occur at the lowest x -value and they decrease when x tends to one. At $x = 0.01$ the order α_s^2 corrections w.r.t. $F_{3,c}^{(1)}$ amount to 14% for $Q^2 = 10 \text{ (GeV/c)}^2$ (Fig. 9) and 20% for $Q^2 = 100 \text{ (GeV/c)}^2$ (Fig. 10). Therefore at increasing Q^2 the corrections get larger. Finally we want to call attention to the difference in behaviour between $F_{2,c}^{(l)}$ and $F_{3,c}^{(l)}$ for $l = 0, 1, 2$. From Figs. 7-10 we infer that $F_{2,c}^{(2)} > F_{2,c}^{(1)} > F_{2,c}^{(0)}$ whereas $F_{3,c}^{(0)} > F_{3,c}^{(2)} > F_{3,c}^{(1)}$.

We will now investigate how accurately one can determine the strange-quark density $s(x, \mu^2)$ from the data obtained for the charged-current [3] and electromagnetic-current [5] interactions. To that order we will compute the ratio in the three-flavour scheme which is defined by

$$R_s^{(l)}(x, Q^2, m^2) = \frac{\Delta^{(l)}(x, Q^2, m^2)}{xs^{(l)}(x, Q^2)} \quad (3.2)$$

with (see also (1.6))

$$\begin{aligned} \Delta^{(l)} = & \frac{5}{12} \left(F_2^{\nu N, (l)} + F_2^{\bar{\nu} N, (l)} + F_{2,c}^{\nu N, (l)} + F_{2,c}^{\bar{\nu} N, (l)} \right) \\ & - 3 \left(F_2^{\mu N, (l)} + F_{2,c}^{\mu N, (l)} \right) \end{aligned} \quad (3.3)$$

where F_2^{lN} , $F_{2,c}^{lN}$ ($l = \nu, \bar{\nu}, \mu$) denote the light-parton contributions ((2.1), (2.14)) and the charm component ((2.7), (2.15)) of the structure functions respectively. For the computation of $F_{2,c}^{\mu N}$ we will use the exact order α_s^2 contributions to the heavy-quark coefficient functions as presented in [21]. Further $s^{(0)}(x, \mu^2)$ and $s^{(1)}(x, \mu^2)$ stand for the LL and NLL parametrizations of the strange-quark density. Since the NNLL parametrization is unknown we have to put $s^{(2)}(x, \mu^2) = s^{(1)}(x, \mu^2)$. The phenomenon that $R_s^{(0)} \not\equiv \emptyset$ can be

only due to the effect of the mass of the charm quark. For $l \geq 1$ one gets in addition deviations which originate from the higher order QCD corrections. We have plotted $R_s^{(l)}$ ($l = 0, 1, 2$) in the range $10^{-4} < x < 1$ for three different Q^2 -values i.e. $Q^2 = 10, 100, 10^4$ (GeV/c)². In Fig. 11 ($Q^2 = 10$ (GeV/c)²) we observe that $R_s^{(0)}$ strongly deviates from one in the region $0.1 < x < 1$, which is wholly due to thresholds effects of the charm quark in $F_{2,c}^{\nu N,(0)}$ and $F_{2,c}^{\bar{\nu} N,(0)}$. This effect will vanish when Q^2 gets larger (see Figs. 12,13). Notice that in the region $x \geq 0.1$ the size of the strange-quark density is very small. For $x < 0.1$ $R_s^{(0)}$ tends to one for $Q^2 > 10$ (GeV/c)². This picture does not change when one includes the order α_s corrections provided $R_s^{(1)}$ is computed at small Q^2 (see Fig. 11). At large Q^2 (see Figs. 12,13), $R_s^{(1)}$ differs appreciably from one in particular at small x . The difference becomes even larger when one includes the order α_s^2 contributions (see $R_s^{(2)}$ in Figs. 11-13). This effect is wholly due to the heavy-quark coefficient functions $H_{2,i}^V$ ($V = \gamma, W$), appearing in the structure functions of (3.3) which grow as $\ln^i(Q^2/m^2)$ when $Q^2 \gg m^2$. Notice that from Fig. 5 one can see that the estimate of the order α_s^2 contributions to $F_{2,c}^{\nu N}$ and $F_{2,c}^{\bar{\nu} N}$ is quite reliable for $Q^2 > 10$ (GeV/c)² and $x < 0.01$. From Figs. 11-13 we can conclude that at small x , $R_s^{(1)}$ and $R_s^{(2)}$ become smaller than 0.5, which means that the actual strange-quark density is more than two times larger than the value obtained for Δ in (3.3). Hence one can conclude that the higher order QCD corrections bedevil the extraction of the strange-quark density in the region $x < 0.1$. Furthermore the effect of the mass of the charm quark is not negligible at small Q^2 ($Q^2 < 10$ (GeV/c)²) in the large x -region ($x \geq 0.1$).

The steep rise of the heavy-quark coefficient functions which grow like $\ln^i(Q^2/m^2)$ for $Q^2 \gg m^2$ becomes even more conspicuous if we study charm production at HERA where one measures the structure functions $F_{k,c}^{\nu e p} (\equiv F_{k,c}^{e^- p})$ and $F_{k,c}^{\bar{\nu} e p} (\equiv F_{k,c}^{e^+ p})$. The latter are plotted for $Q^2 = 10^4$ (GeV/c)² in the region $0.006 < x < 0.5$ in Figs. 14-17. In this kinematical region the approximations to the second order heavy-quark coefficient functions become excellent (see Figs. 3-6). This already happens at the lowest Q^2 -value i.e. $Q^2 = 200$ (GeV/c)² measured in [16]. In the case of $F_{2,c}$ the exact order α_s^2 corrections are not that spectacular and they amount to almost 7% at $x = 0.006$ w.r.t. to $F_{2,c}^{(1)}$ (see Figs. 14,15). This is in contrast to $F_{3,c}$ (see Figs. 16,17) where the order α_s^2 corrections become 32% w.r.t. $F_{3,c}^{(1)}$ (see Fig. 17). These large corrections, occurring at small x and large Q^2 ,

vitiates the perturbation series in particular the one given for $F_{3,c}$. Therefore the large logarithmic terms represented by $\ln^i(Q^2/m^2)$ have to be resummed according to the VFNS approach (see [11], [20]). In the latter scheme the charm component of the structure functions takes the following form

$$F_{k,c}^{W^+p}(x, Q^2) \equiv F_{k,c}^{\nu p}(x, Q^2) = a_k(x) \int_x^1 \frac{dz}{z} \left[\Sigma_4\left(\frac{x}{z}, \mu^2\right) \tilde{C}_{k,q}^{\text{PS}}\left(z, \frac{Q^2}{\mu^2}\right) + G\left(\frac{x}{z}, \mu^2\right) \tilde{C}_{k,g}^{\text{S}}\left(z, \frac{Q^2}{\mu^2}\right) + \left\{ b_{k,\bar{c}}\left(\frac{x}{z}, \mu^2\right) + b_{k,d} \sin^2(\theta_C) d\left(\frac{x}{z}, \mu^2\right) + b_{k,s} \cos^2(\theta_C) s\left(\frac{x}{z}, \mu^2\right) \right\} \mathcal{C}_{k,q}^{\text{NS}}\left(z, \frac{Q^2}{\mu^2}\right) \right] \quad (3.4)$$

where the parton densities and the light-quark coefficient functions $\mathcal{C}_{k,i}$ ($k = 2, 3; i = q, g$) are presented in the four-flavour scheme. The parton-density set now also contains the charm-quark density $c(z, \mu^2)$ and the singlet combination reads

$$\Sigma_4(z, \mu^2) = \Sigma_3(z, \mu^2) + c(z, \mu^2) + \bar{c}(z, \mu^2) \quad (3.5)$$

where $\Sigma_3(z, \mu^2)$ is defined in (2.4). The structure function $F_{k,c}^{\bar{\nu}p}$ ($\equiv F_{k,c}^{W^-p}$) can be derived by interchanging quarks and anti-quarks (see below (2.9)). In order to compute (3.4) we need the charm-quark density which however is not present in GRV94 [25] because the latter set is presented in a three-flavour scheme. Therefore we have adopted GRV92 [27] with $\Lambda_4^{(\text{LO})} = \Lambda_4^{(\text{NLO})} = 200$ MeV which contains the charm-quark density. We first checked that using the densities in GRV92 for the expressions in the three-flavour scheme one gets the same results for $F_{2,c}$ as obtained with GRV94. In the case of $|F_{3,c}|$, the latter set produces values which are 10% below those given by GRV92. As a comparison we have also plotted in Figs. 14-17 $F_{k,c}^{(1)}$ (VFNS) using Eq. (3.4) and GRV92. It turns out that the result for $F_{2,c}^{(1)}$ is larger in VFNS (3.4) than obtained by FFS (see Figs. 14,15). This observation was also made in [13]. The discrepancy becomes less when the order α_s^2 corrections are included in the case of FFS (see $F_{2,c}^{(2)}$). This feature was also discovered for $F_{2,c}^{ep}$ in the electromagnetic-current process [20]. However, for $F_{3,c}$ the difference between

the two schemes is large (see Figs. 16,17), in particular in the small x -region. Here we observe that $F_{3,c}^{(1)}$ in VFNS deviates appreciably from $F_{3,c}^{(1)}$ as well as $F_{3,c}^{(2)}$ in FFS. This is no surprise because, as we have seen above, in FFS the large logarithms in the heavy-quark coefficient functions lead to larger corrections to $F_{3,c}$ than to $F_{2,c}$. Therefore the resummation of these terms will have a larger effect on $F_{3,c}$ than on $F_{2,c}$. This is the explanation of the difference between the predictions of the FFS and VFNS approach for the HERA experiments as originally observed for $F_{2,c}^{(1)}$ in [13]. Since we believe that the resummation of these large logarithmic terms has to be carried out for $Q^2 \gg m^2$, the results obtained by Eq. (3.4) (VFNS) are much more reliable than those obtained in FFS given by the expressions in Section 2.

Summarizing our findings, we have studied the effect of the order α_s^2 contributions from the heavy-quark coefficient functions to the charm component of the charged-current structure functions. Since for some of them the exact expressions do not exist we have to rely on approximations which are strictly speaking valid only for $Q^2 \gg m^2$ (HERA-regime). However, from a comparison based on the exact and asymptotic order α_s heavy-quark coefficient functions corresponding to the W-boson-gluon fusion process, the predictions are also reliable for $Q^2 > 20 \text{ (GeV/c)}^2$ and $x < 0.08$. At smaller x it is even sufficient to choose $Q^2 > 10 \text{ (GeV/c)}^2$.

The outcome of our analysis reveals that the order α_s^2 corrections are small for $F_{2,c}$ but large for $F_{3,c}$, in particular when Q^2 is big. These large corrections are due to the logarithmic terms $\ln^i(Q^2/m^2)$ dominating the heavy-quark coefficient functions characteristic of the FFS approach. Therefore at large Q^2 these terms have to be resummed in the context of VFNS, leading to a better prediction, in particular for $F_{3,c}$. Finally we want to stress that the higher order QCD corrections bedevil the extraction of the strange-quark density from the charged- and electromagnetic-current total structure functions, in particular at small x ($x < 0.08$).

Appendix A

In this section we will derive the relations between the heavy-quark coefficient functions $H_{k,i}^W$ and $H_{2,i}^\gamma$ ($k = 2, 3; i = q, g$) obtained for the charged-current and the electromagnetic-current processes respectively. Using mass-factorization techniques one has shown in [17]-[20] that there exists a relation between the asymptotic ($Q^2 \gg m^2$) heavy-quark coefficient functions $H_{k,i}^V$ and the light-parton coefficient functions $\mathcal{C}_{k,i}$. Hence one can derive that up to order α_s^2 the heavy-quark coefficient functions corresponding to the reactions

$$i + V \rightarrow q_1 + \bar{q}_2, \quad (\text{A.1})$$

$$i + V \rightarrow q_1 + \bar{q}_2 + j, \quad (\text{A.2})$$

in the asymptotic limit $Q^2 \gg m^2$ can be written as (see Eqs. (2.34), (2.35) in [20])

$$\begin{aligned} H_{k,i}^V \left(\frac{Q^2}{m_1^2}, \frac{Q^2}{m_2^2}, \frac{m_1^2}{\mu^2}, \frac{m_2^2}{\mu^2} \right) &= \frac{1}{2} A_{q_1 i} \left(\frac{m_1^2}{\mu^2} \right) \otimes \mathcal{C}_{k,q_1}^S \left(\frac{Q^2}{\mu^2} \right) \\ &+ \frac{1}{2} A_{\bar{q}_2 i} \left(\frac{m_2^2}{\mu^2} \right) \otimes \mathcal{C}_{k,\bar{q}_2}^S \left(\frac{Q^2}{\mu^2} \right) + \frac{1}{2} A_{gi} \left(\frac{m_1^2}{\mu^2} \right) \otimes \tilde{\mathcal{C}}_{k,g}^S \left(\frac{Q^2}{\mu^2} \right) \\ &+ \frac{1}{2} A_{gi} \left(\frac{m_2^2}{\mu^2} \right) \otimes \tilde{\mathcal{C}}_{k,g}^S \left(\frac{Q^2}{\mu^2} \right). \end{aligned} \quad (\text{A.3})$$

For convenience we have suppressed the Bjorken scaling variable $z = Q^2/2p_i q$ and \otimes denotes the convolution symbol defined by

$$(f \otimes g)(z) = \int_0^1 dz_1 \int_0^1 dz_2 \delta(z - z_1 z_2) f(z_1) g(z_2). \quad (\text{A.4})$$

The light partons involved in reactions (A.1) and (A.2) are given by i and j ($i, j = q, g$). For $V = \gamma$ both q_1 and q_2 stand for the heavy quarks whereas for $V = W$ one of them is represented by a light quark. The masses of q_1 and q_2 are given by m_1 and m_2 respectively. The light-parton coefficient functions $\mathcal{C}_{k,i}$ ($i = q, g$) are obtained from the massless-parton subprocesses

$$i + V \rightarrow j_1 + j_2 + \dots + j_k \quad (\text{A.5})$$

which are independent of the nature of the probe V . Further when the quarks q_1 and q_2 in (A.3) are massless the coefficient functions satisfy the relation $\mathcal{C}_{k,q_1}^S = \mathcal{C}_{k,q_2}^S$. The light parton coefficient functions in (A.3) are calculated up to order α_s^2 in [23]. Expression (A.3) requires the knowledge of the renormalized heavy-quark operator matrix elements (OME's)

$$A_{qi}\left(\frac{m_l^2}{\mu^2}\right) = \langle i | O_{qi}(0) | i \rangle \quad (\text{A.6})$$

and the heavy-quark loop contributions to the renormalized light-parton OME's given by

$$A_{ji}\left(\frac{m_l^2}{\mu^2}\right) = \langle i | O_j(0) | i \rangle \quad (\text{A.7})$$

with

$$A_{ji}^{(0)}\left(z, \frac{m_l^2}{\mu^2}\right) = \delta_{ji} \delta(1-z). \quad (\text{A.8})$$

The above OME's are calculated up to order α_s^2 in [17] and the renormalized expressions are presented in the $\overline{\text{MS}}$ -scheme in Appendix B of [20]. Furthermore they satisfy the conditions when $m_l^2 = 0$

$$A_{qi}(0) = 0, \quad A_{ji}(z, 0) = \delta_{ji} \delta(1-z). \quad (\text{A.9})$$

The local operators $O_j(x)$ appear in the light-cone expansion of the product of the two electroweak currents which, after having taken the Fourier transform, show up in the expressions for the structure functions $F_k(x, Q^2)$ (see [28]).

In the case of $V = \gamma$ Eq. (A.3) leads in the first and second order to the following relations ($m_1 = m_2 = m; q_1 = q_2 = c$)

$$H_{2,g}^{\gamma,(1)}\left(\frac{Q^2}{m^2}, \frac{m^2}{\mu^2}\right) = A_{cg}^{(1)}\left(\frac{m^2}{\mu^2}\right) + \tilde{\mathcal{C}}_{2,g}^{\text{S},(1)}\left(\frac{Q^2}{\mu^2}\right), \quad (\text{A.10})$$

$$\begin{aligned} H_{2,g}^{\gamma,(2)}\left(\frac{Q^2}{m^2}, \frac{m^2}{\mu^2}\right) &= A_{cg}^{(2)}\left(\frac{m^2}{\mu^2}\right) + A_{cg}^{(1)}\left(\frac{m^2}{\mu^2}\right) \otimes \mathcal{C}_{2,q}^{\text{NS},(1)}\left(\frac{Q^2}{\mu^2}\right) \\ &\quad + \tilde{\mathcal{C}}_{2,g}^{\text{S},(2)}\left(\frac{Q^2}{\mu^2}\right), \end{aligned} \quad (\text{A.11})$$

$$H_{2,q}^{\gamma,\text{PS},(2)}\left(\frac{Q^2}{m^2}, \frac{m^2}{\mu^2}\right) = A_{cq}^{\text{PS},(2)}\left(\frac{m^2}{\mu^2}\right) + \tilde{\mathcal{C}}_{2,q}^{\text{PS},(2)}\left(\frac{Q^2}{\mu^2}\right), \quad (\text{A.12})$$

where we have expanded all quantities up to order $(\alpha_s^2/4\pi)^2$. Notice that in the case of $V = \gamma$, $H_{3,i}^\gamma = 0$. Furthermore $\mathcal{C}_{i,c} = \mathcal{C}_{i,q}$ when $m \rightarrow 0$.

For $V = W$ the above relations become ($m_1 = m, m_2 = 0; q_1 = c, q_2 = d, s$)

$$H_{2,g}^{W,(1)}\left(\frac{Q^2}{m^2}, \frac{m^2}{\mu^2}\right) = \frac{1}{2}A_{cg}^{(1)}\left(\frac{m^2}{\mu^2}\right) + \tilde{\mathcal{C}}_{2,g}^{\text{S},(1)}\left(\frac{Q^2}{\mu^2}\right), \quad (\text{A.13})$$

$$\begin{aligned} H_{2,g}^{W,(2)}\left(\frac{Q^2}{m^2}, \frac{m^2}{\mu^2}\right) &= \frac{1}{2}A_{cg}^{(2)}\left(\frac{m^2}{\mu^2}\right) + \frac{1}{2}A_{cg}^{(1)}\left(\frac{m^2}{\mu^2}\right) \otimes \mathcal{C}_{2,q}^{\text{NS},(1)}\left(\frac{Q^2}{\mu^2}\right) \\ &\quad + \tilde{\mathcal{C}}_{2,g}^{\text{S},(2)}\left(\frac{Q^2}{\mu^2}\right), \end{aligned} \quad (\text{A.14})$$

$$H_{2,q}^{W,\text{PS},(2)}\left(\frac{Q^2}{m^2}, \frac{m^2}{\mu^2}\right) = \frac{1}{2}A_{cq}^{\text{PS},(2)}\left(\frac{m^2}{\mu^2}\right) + \tilde{\mathcal{C}}_{2,q}^{\text{PS},(2)}\left(\frac{Q^2}{\mu^2}\right). \quad (\text{A.15})$$

For the heavy-quark coefficient functions $H_{3,i}^W$ we have to use the following relations

$$\mathcal{C}_{3,q}^{\text{NS}} = -\mathcal{C}_{3,\bar{q}}^{\text{NS}}, \quad \tilde{\mathcal{C}}_{3,g}^{\text{S}} = 0, \quad \tilde{\mathcal{C}}_{3,q}^{\text{PS}} = 0 \quad (\text{A.16})$$

which follow from charge conjugation invariance of the strong interactions. Hence we can derive from Eq. (A.3)

$$H_{3,g}^{W,(1)}\left(\frac{Q^2}{m^2}, \frac{m^2}{\mu^2}\right) = \frac{1}{2}A_{cg}^{(1)}\left(\frac{m^2}{\mu^2}\right), \quad (\text{A.17})$$

$$H_{3,g}^{W,(2)}\left(\frac{Q^2}{m^2}, \frac{m^2}{\mu^2}\right) = \frac{1}{2}A_{cg}^{(2)}\left(\frac{m^2}{\mu^2}\right) + \frac{1}{2}A_{cg}^{(1)}\left(\frac{m^2}{\mu^2}\right) \otimes \mathcal{C}_{3,q}^{\text{NS},(1)}\left(\frac{Q^2}{\mu^2}\right), \quad (\text{A.18})$$

$$H_{3,q}^{W,\text{PS},(2)}\left(\frac{Q^2}{m^2}, \frac{m^2}{\mu^2}\right) = \frac{1}{2}A_{cq}^{\text{PS},(2)}\left(\frac{m^2}{\mu^2}\right). \quad (\text{A.19})$$

Similar relations can be derived when $m_1 = 0, m_2 = m$ and $q_1 = d, s; q_2 = c$. Using Eqs. (A.10)-(A.12) one can now express $H_{k,i}^W$ into $H_{k,i}^\gamma$. The results are presented in (2.17)-(2.19).

References

- [1] S.A. Rabinowitz et al., Phys. Rev. Lett. **70** (1993) 134.
- [2] A.O. Bazarko et al. (CCFR-collaboration), Z. Phys. **C65** (1995) 189.
- [3] E. Oltman et al. (CCFR-collaboration), Z. Phys. **C53** (1992) 51.
- [4] CCFR-collaboration, talk presented at the 1991 SLAC Summer School on Lepton-Hadron Scattering.
- [5] M. Arneodo et al. (NMC-collaboration), Phys. Lett. **B364** (1995) 107.
- [6] M. Glück, S. Kretzer, E. Reya, Phys. Lett. **B380** (1996) 171.
- [7] Th. Gottschalk, Phys. Rev. **D23** (1981) 56.
- [8] J.J. van der Bij and G.J. van Oldenborgh, Z. Phys. **C51** (1991) 477.
- [9] G. Kramer and B. Lampe, Z. Phys. **C54** (1992) 139.
- [10] M. Glück, E. Hoffmann and E. Reya, Z. Phys. **C13** (1982) 119.
M. Glück, R.M. Godbole and E. Reya, Z. Phys. **C38** (1988) 441.
- [11] M.A.G. Aivazis, J.C. Collins, F.I. Olness and W.-K. Tung, Phys. Rev. **D50** (1994) 3102.
- [12] G. Kramer, B. Lampe and H. Spiesberger, Z. Phys. **C72** (1996) 99.
- [13] V. Barone, U. D'Alesio and M. Genovese, hep-ph/9610211.
- [14] T. Ahmed et al. (H1-collaboration), Phys. Lett. **B324** (1994) 241.
- [15] S. Aid et al. (H1-collaboration), Z. Phys. **C67** (1995) 565; *ibid.* Phys. Lett. **B379** (1996) 319.
- [16] M. Derrick et al. (ZEUS-collaboration), Phys. Rev. Lett. **75** (1995) 1006; *ibid.* Z. Phys. **C72** (1996) 47, *ibid.* Z. Phys. **C72** 399.
- [17] M. Buza, Y. Matiounine, J. Smith, R. Migneron and W.L. van Neerven, Nucl. Phys. **B472** (1996) 611, *ibid.* Nucl. Phys. B (Proc. Suppl.) **51C** (1996) 183.

- [18] M. Buza, Y. Matiounine, J. Smith, W.L. van Neerven, hep-ph/9608342, to be published in Nucl. Phys. B.
- [19] M. Buza et al. , Proceedings of the Workshop "Future Physics at HERA", DESY, Hamburg 1995/1996, 393.
- [20] M. Buza, Y. Matiounine, J. Smith, W.L. van Neerven, hep-ph/9612398.
- [21] E. Laenen, S. Riemersma, J. Smith and W.L. van Neerven, Nucl. Phys. **B392** (1993) 162.
S. Riemersma, J. Smith and W.L. van Neerven, Phys. Lett. **B347** (1995) 143.
B.W. Harris and J. Smith, Nucl. Phys. **B452** (1995) 109.
- [22] W. Furmanski and R. Petronzio, Z. Phys. **C11** (1982) 293.
- [23] E.B. Zijlstra and W.L. van Neerven, Nucl. Phys. **B383** (1992) 525.
- [24] T. van Ritbergen, Phd thesis, University of Amsterdam, 1996.
- [25] M. Glück, E. Reya and A. Vogt, Z. Phys. **C67** (1995) 433.
- [26] R.M. Barnett et al., Review of Particle Physics, PART 1, Phys. Rev **D54** (1996) 94.
- [27] M. Glück, E. Reya and A. Vogt, Z. Phys. **C53** (1992) 127.
- [28] H.D. Politzer, Phys. Rep. **14C** (1974) 129.

Figure Captions

Fig. 1. The order α_s contributions to $F_{2,c}^{\nu N}$ (2.7) due to flavour excitation : $F_{2,c}^q$ (1.4) and W -boson-gluon fusion : $F_{2,c}^g$ (1.5);
solid line: $F_{2,c}^q$ at $Q^2 = 10$ (GeV/c)², dotted line: $F_{2,c}^q$ at $Q^2 = 100$ (GeV/c)², dashed line: $F_{2,c}^g$ at $Q^2 = 10$ (GeV/c)², dashed-dotted line: $F_{2,c}^g$ at $Q^2 = 100$ (GeV/c)².

Fig. 2. Same as Fig. 1 but now for $F_{3,c}^{\nu N}$ (2.7) plotted in absolute value.

Fig. 3. $R_{2,c}$ (3.1) plotted as a function of Q^2 at fixed x ;
 $x = 10^{-1}$ (dotted line), $x = 10^{-2}$ (dashed-dotted line), $x = 10^{-3}$ (dashed line) and $x = 10^{-4}$ (solid line).

Fig. 4. Same as Fig. 3 but now for $R_{3,c}$ (3.1).

Fig. 5. $R_{2,c}$ (3.1) plotted as a function of x at fixed Q^2 ;
 $Q^2 = 10$ (GeV/c)² (dotted line), $Q^2 = 20$ (GeV/c)² (dashed-dotted line), $Q^2 = 50$ (GeV/c)² (dashed line), $Q^2 = 100$ (GeV/c)² (solid line).

Fig. 6. Same as Fig. 5 but now for $R_{3,c}$ (3.1).

Fig. 7. The order α_s^l corrected structure function $F_{2,c}^{\nu N}$ (2.7), denoted by $F_{2,c}^{(l)}$, as a function of x at $Q^2 = 10$ (GeV/c)²;
dotted line : $F_{2,c}^{(0)}$, dashed line : $F_{2,c}^{(1)}$, solid line : $F_{2,c}^{(2)}$.

Fig. 8. Same as Fig. 7 but now at $Q^2 = 100$ (GeV/c)².

Fig. 9. Same as Fig. 7 but now for $F_{3,c}^{\nu N}$ (2.7) at $Q^2 = 10$ (GeV/c)².

Fig. 10. Same as Fig. 7 but now for $F_{3,c}^{\nu N}$ (2.7) at $Q^2 = 100$ (GeV/c)².

Fig. 11. The order α_s^l corrected ratio R_s (3.2), denoted by $R_s^{(l)}$, as a function of x at $Q^2 = 10 \text{ (GeV/c)}^2$;
solid line : $R_s^{(0)}$, dashed line : $R_s^{(1)}$, dotted line : $R_s^{(2)}$.

Fig. 12 Same as Fig. 11 but now at $Q^2 = 100 \text{ (GeV/c)}^2$.

Fig. 13 Same as Fig. 11 but now at $Q^2 = 10^4 \text{ (GeV/c)}^2$.

Fig. 14 The order α_s^l corrected structure function $F_{2,c}^{e^-p} (\equiv F_{2,c}^{\bar{\nu}ep})$ (2.7), denoted by $F_{2,c}^{(l)}$, as a function of x at $Q^2 = 10^4 \text{ (GeV/c)}^2$;
dotted line : $F_{2,c}^{(0)}$ (FFS), dashed line : $F_{2,c}^{(1)}$ (FFS), solid line : $F_{2,c}^{(2)}$ (FFS). As a comparison we have also shown dashed-dotted line : $F_{2,c}^{(1)}$ (VFNS).

Fig. 15 Same as Fig. 14 but now for $F_{2,c}^{e^+p} (\equiv F_{2,c}^{\nu ep})$ (2.7).

Fig. 16 Same as Fig. 14 but now for $F_{3,c}^{e^-p} (\equiv F_{2,c}^{\bar{\nu}ep})$ (2.7).

Fig. 17 Same as Fig. 14 but now for $F_{3,c}^{e^+p} (\equiv F_{2,c}^{\nu ep})$ (2.7).

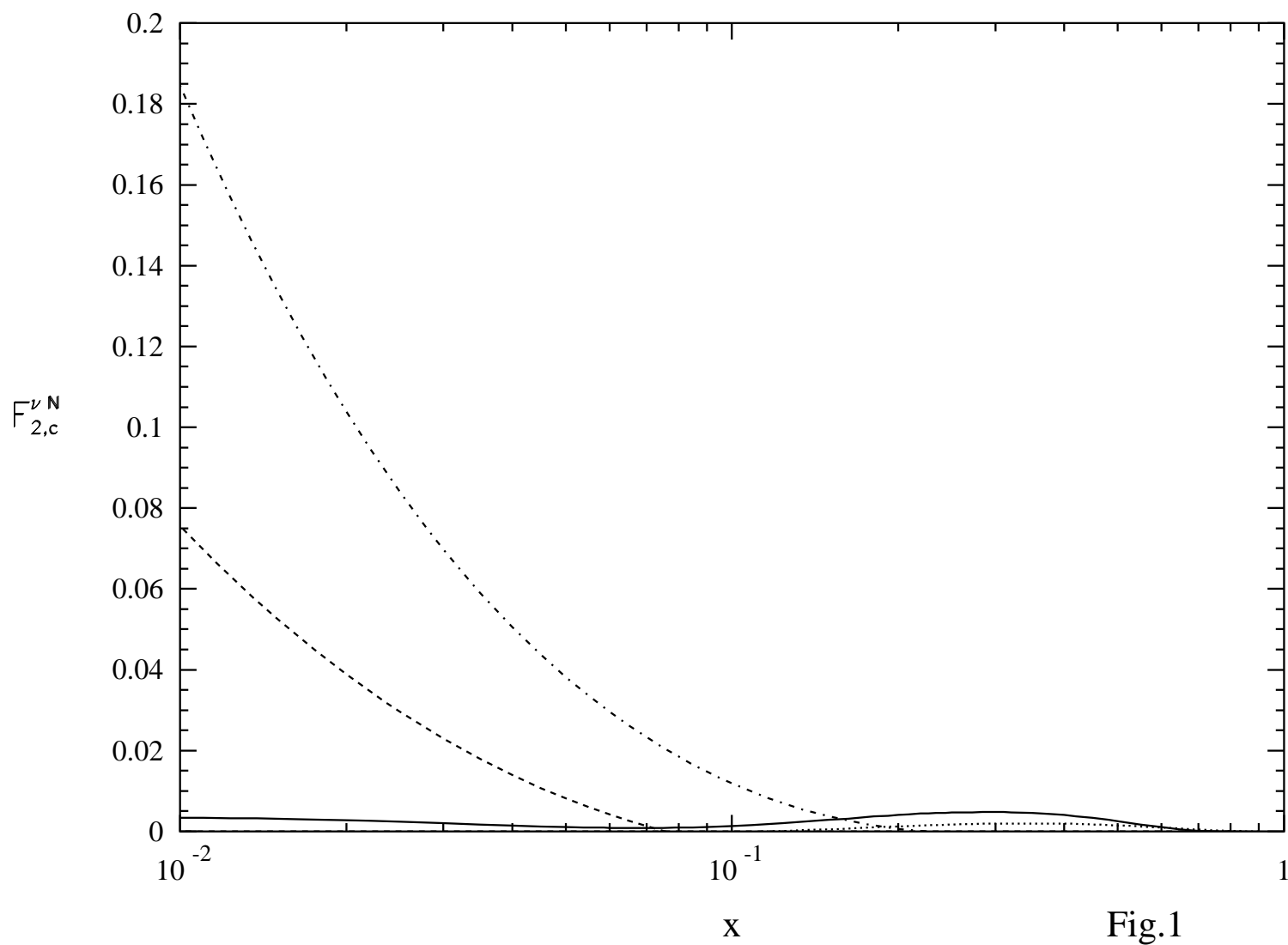


Fig.1

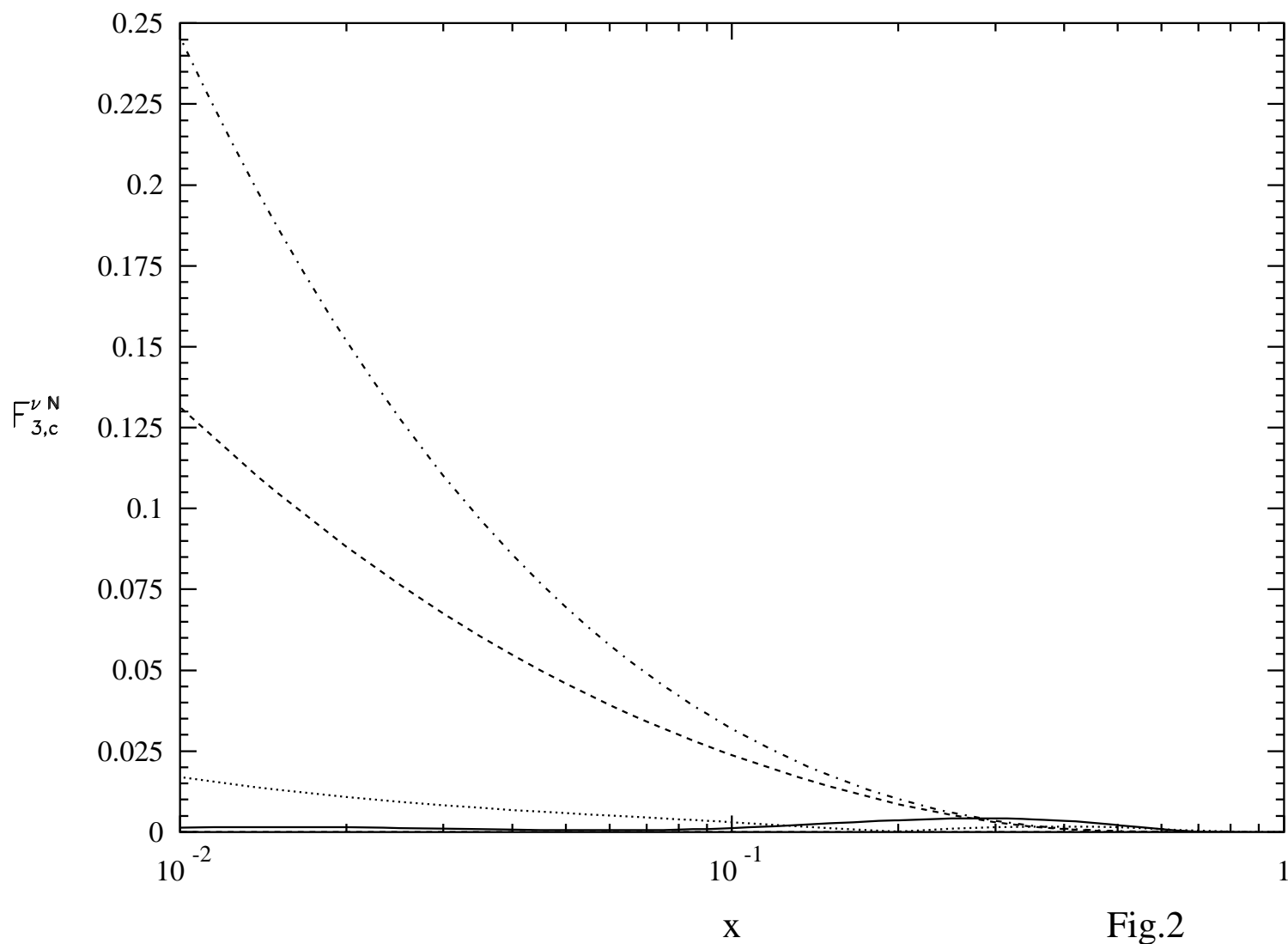


Fig.2

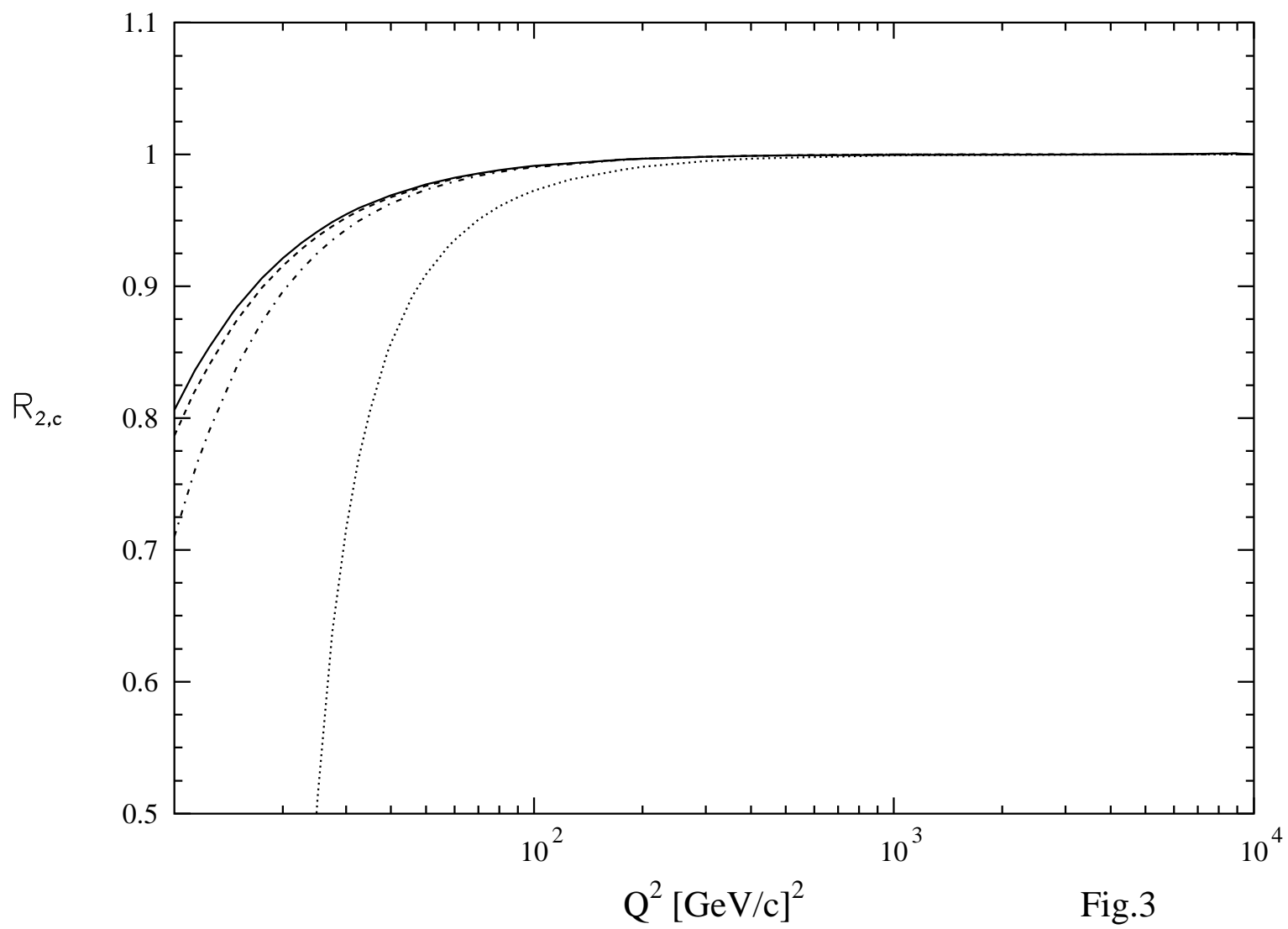


Fig.3

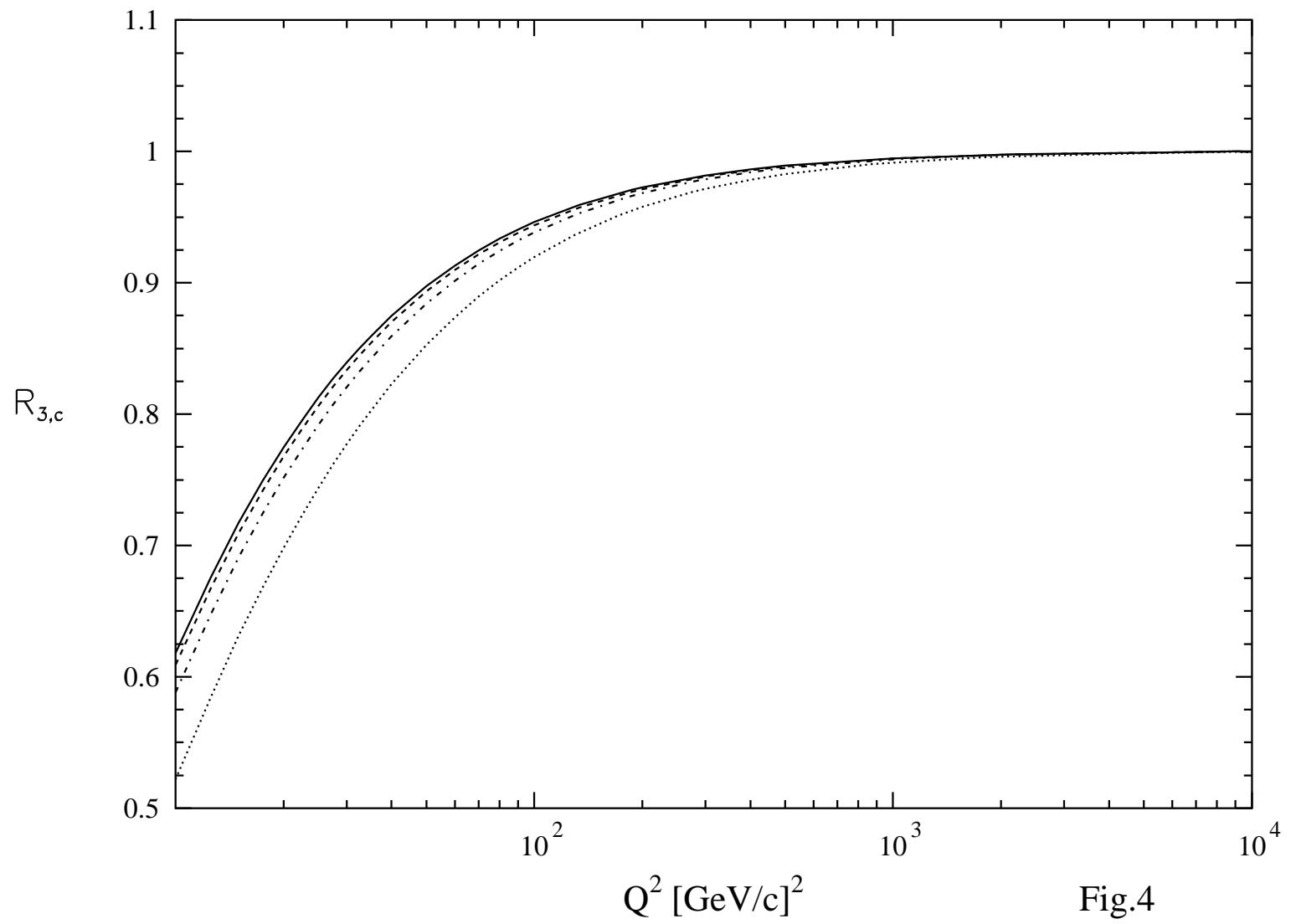


Fig.4

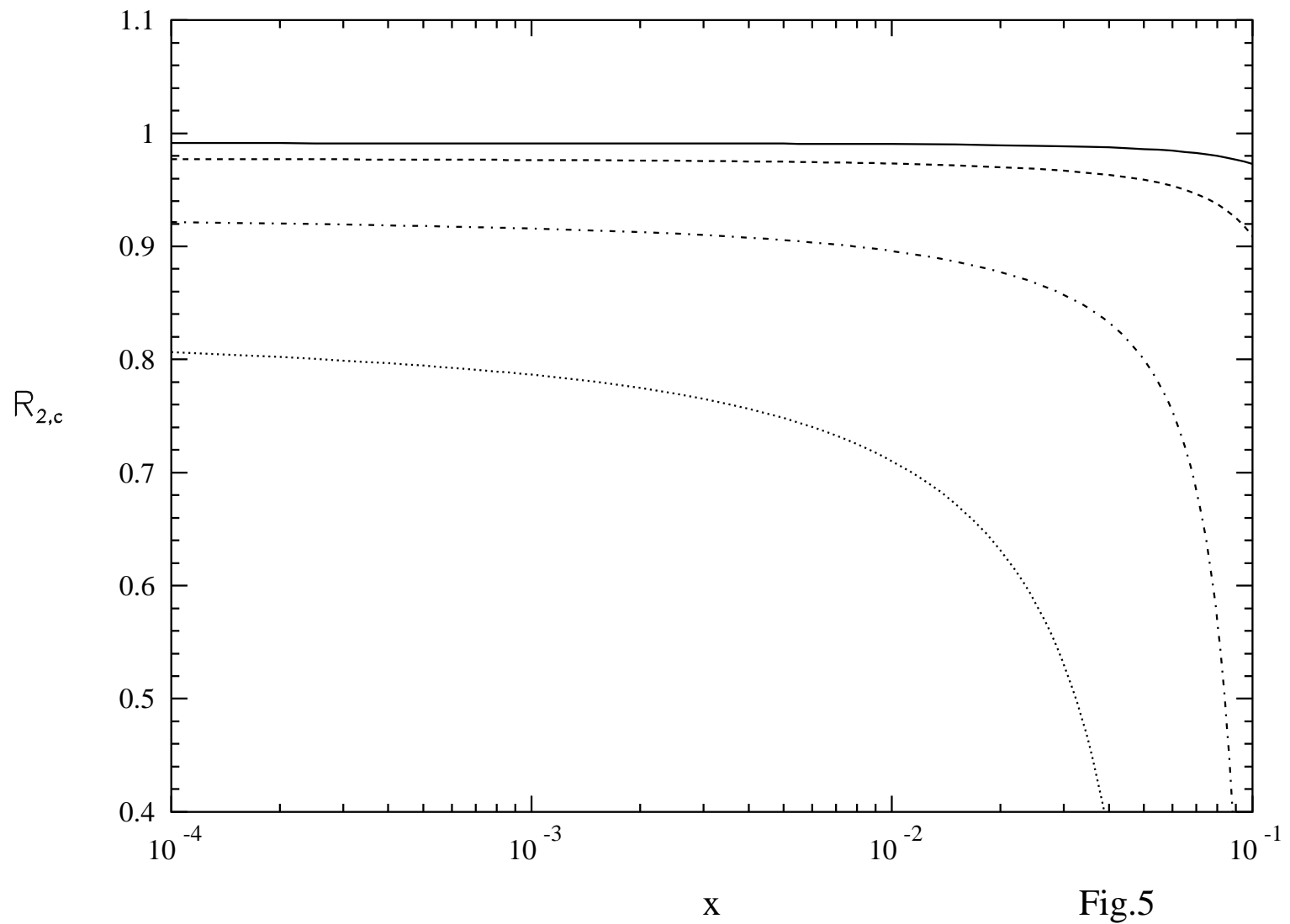


Fig.5

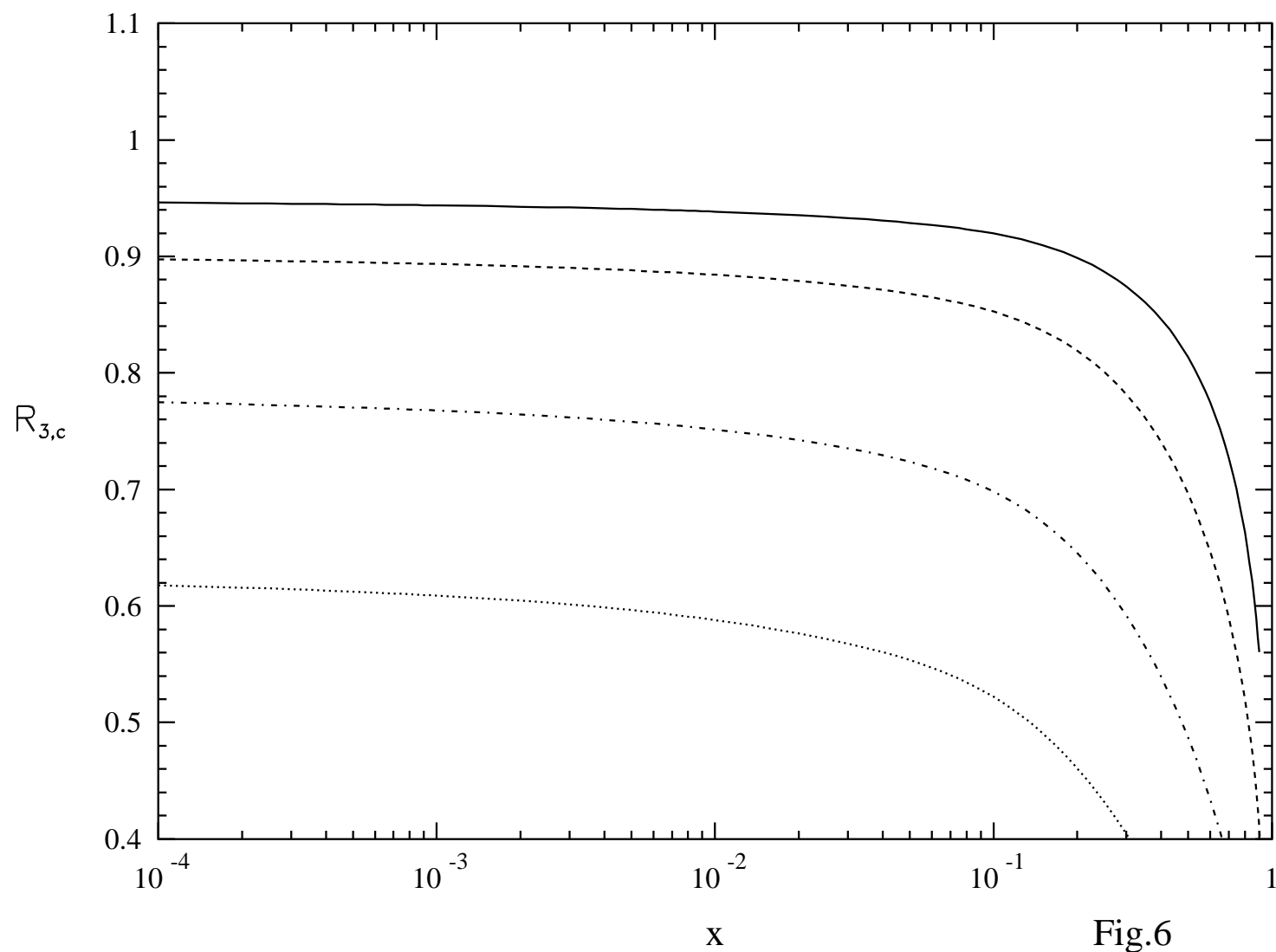


Fig.6

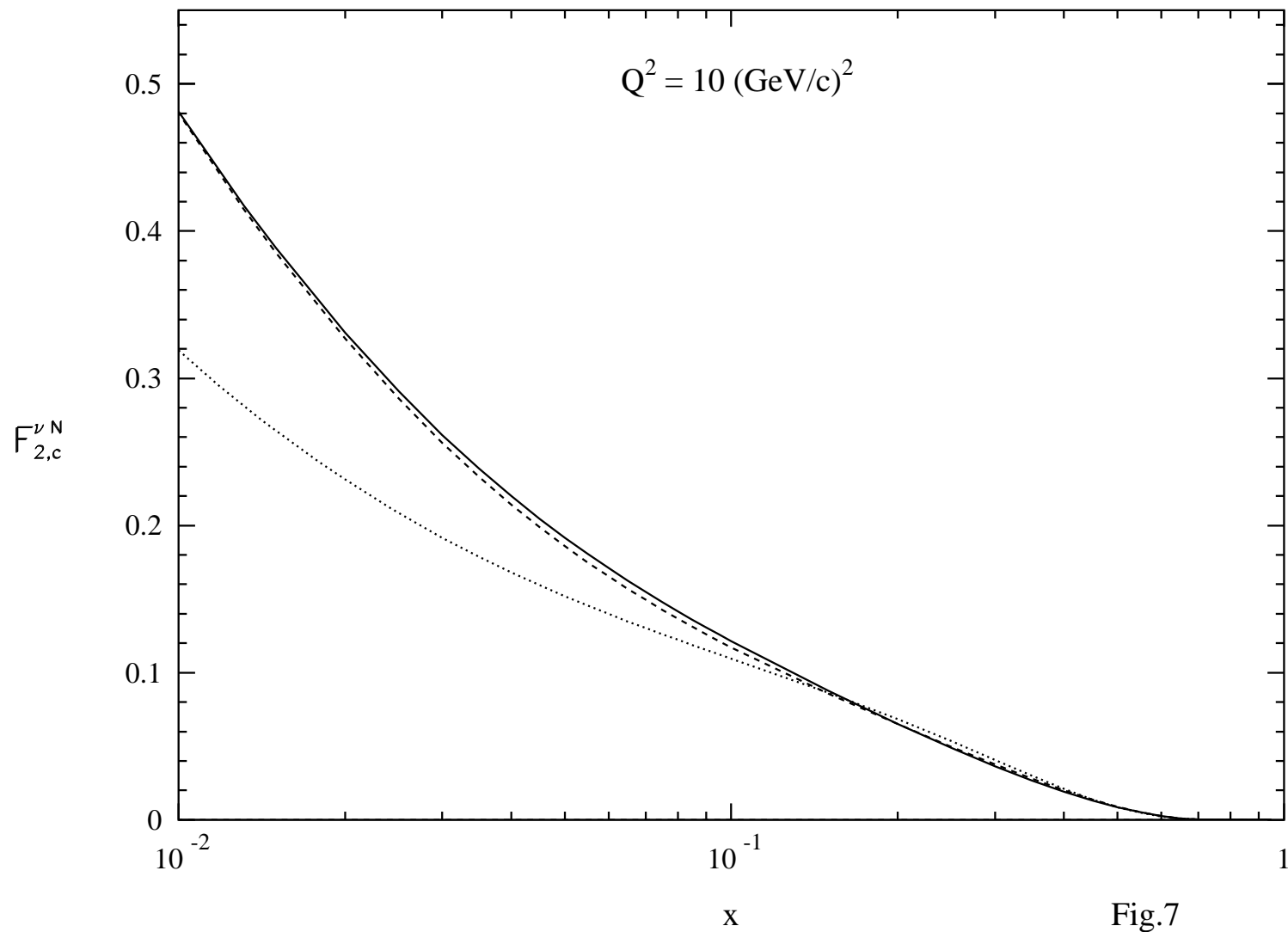


Fig.7

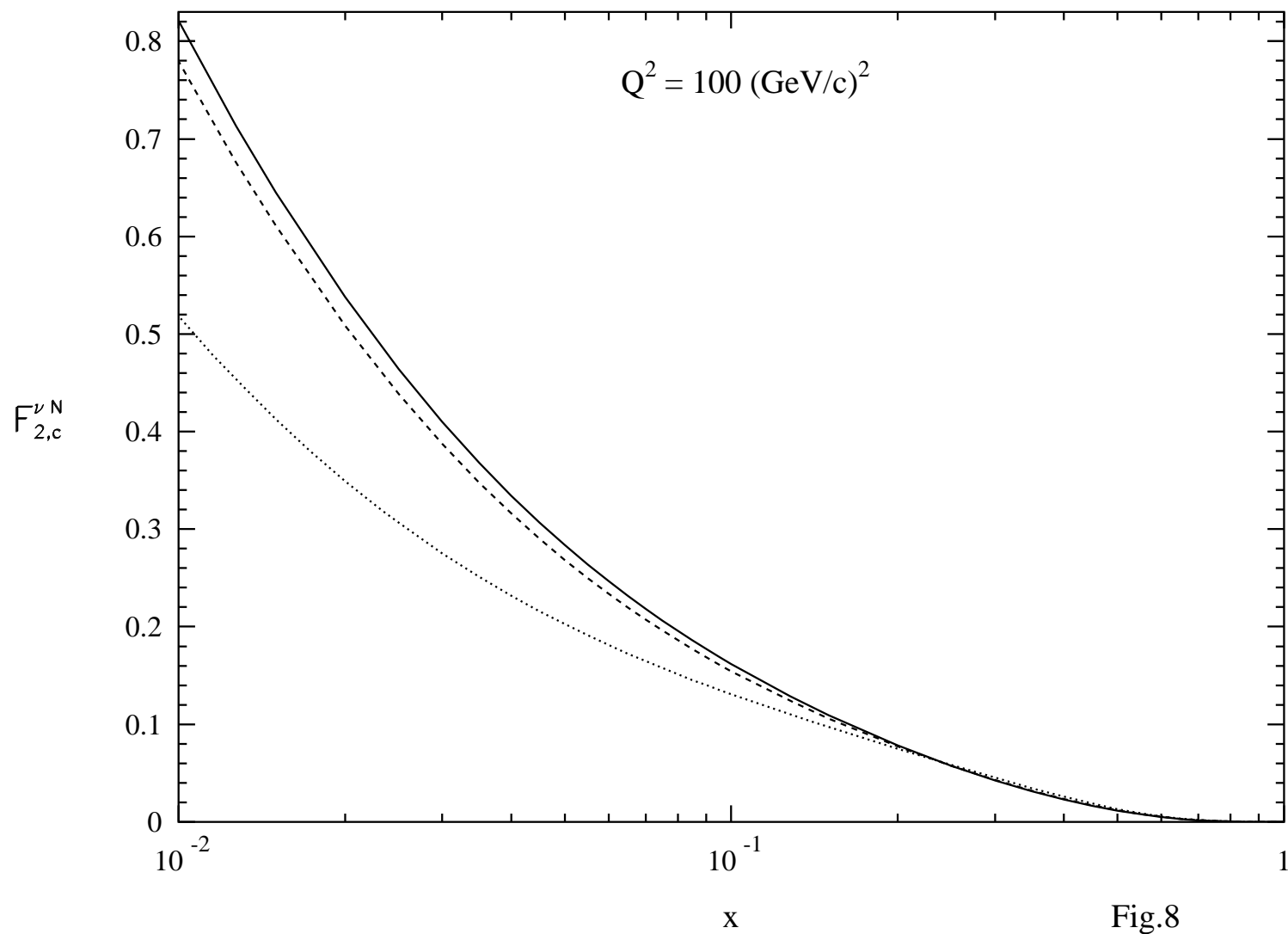


Fig.8

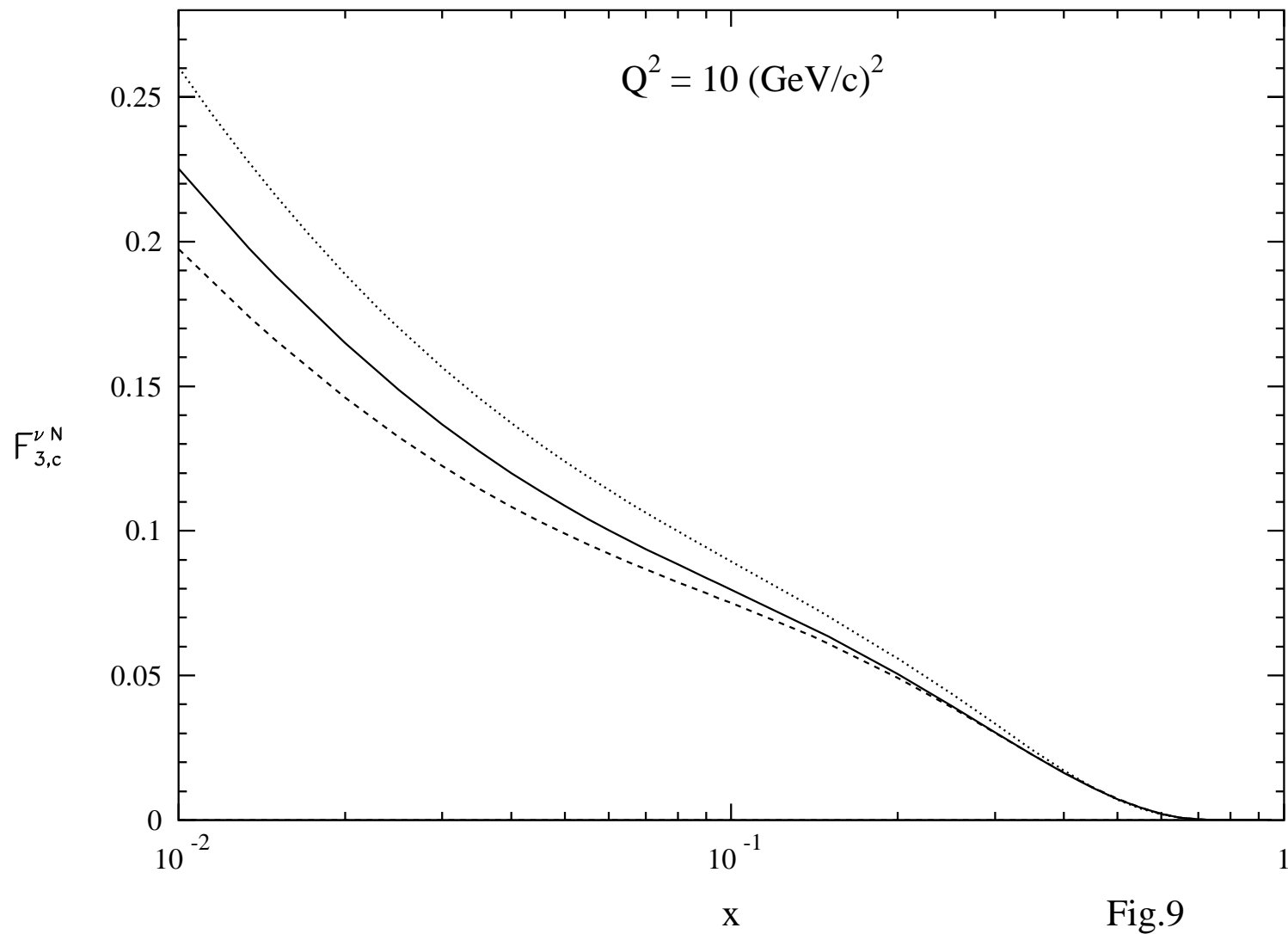
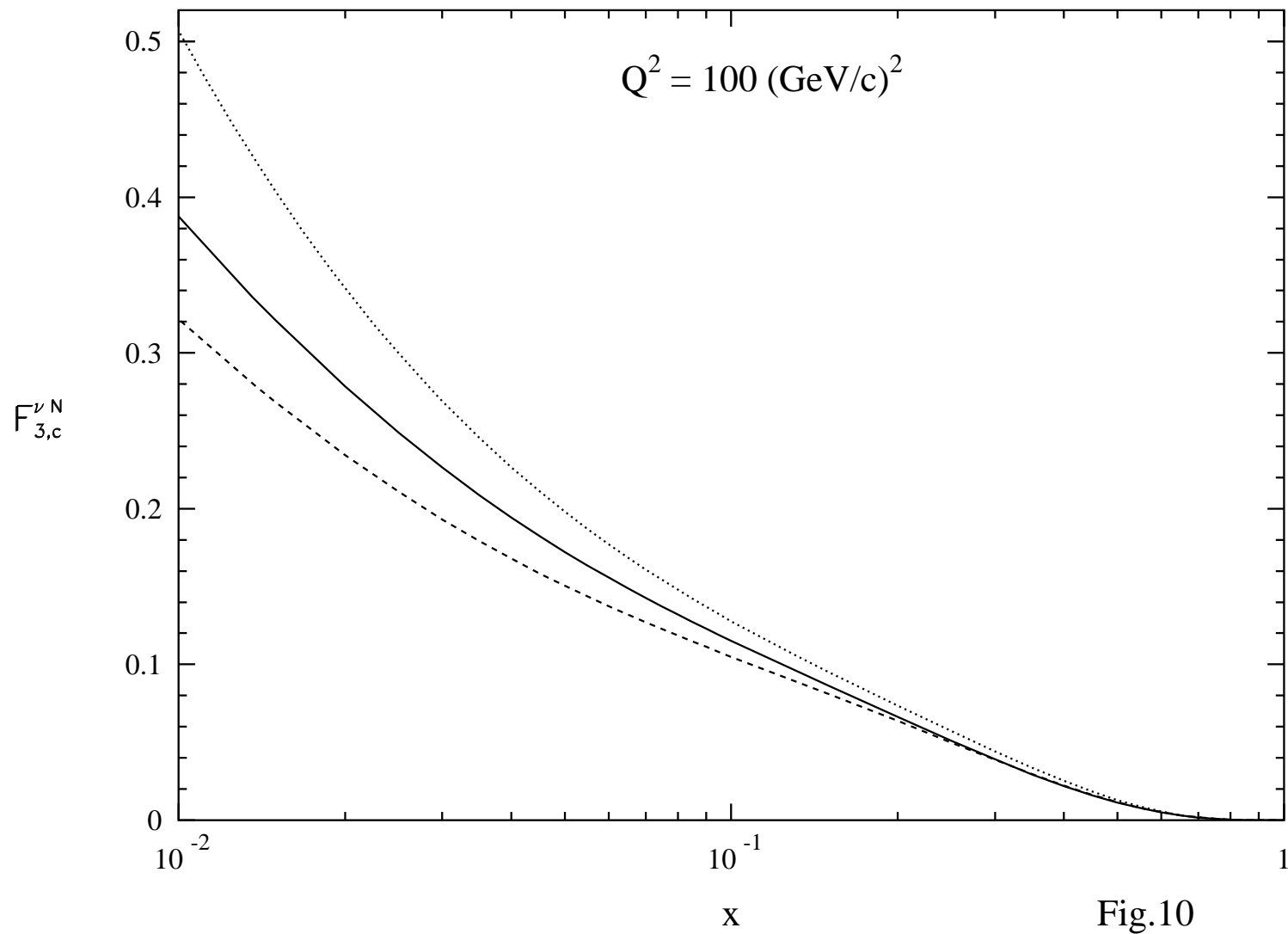
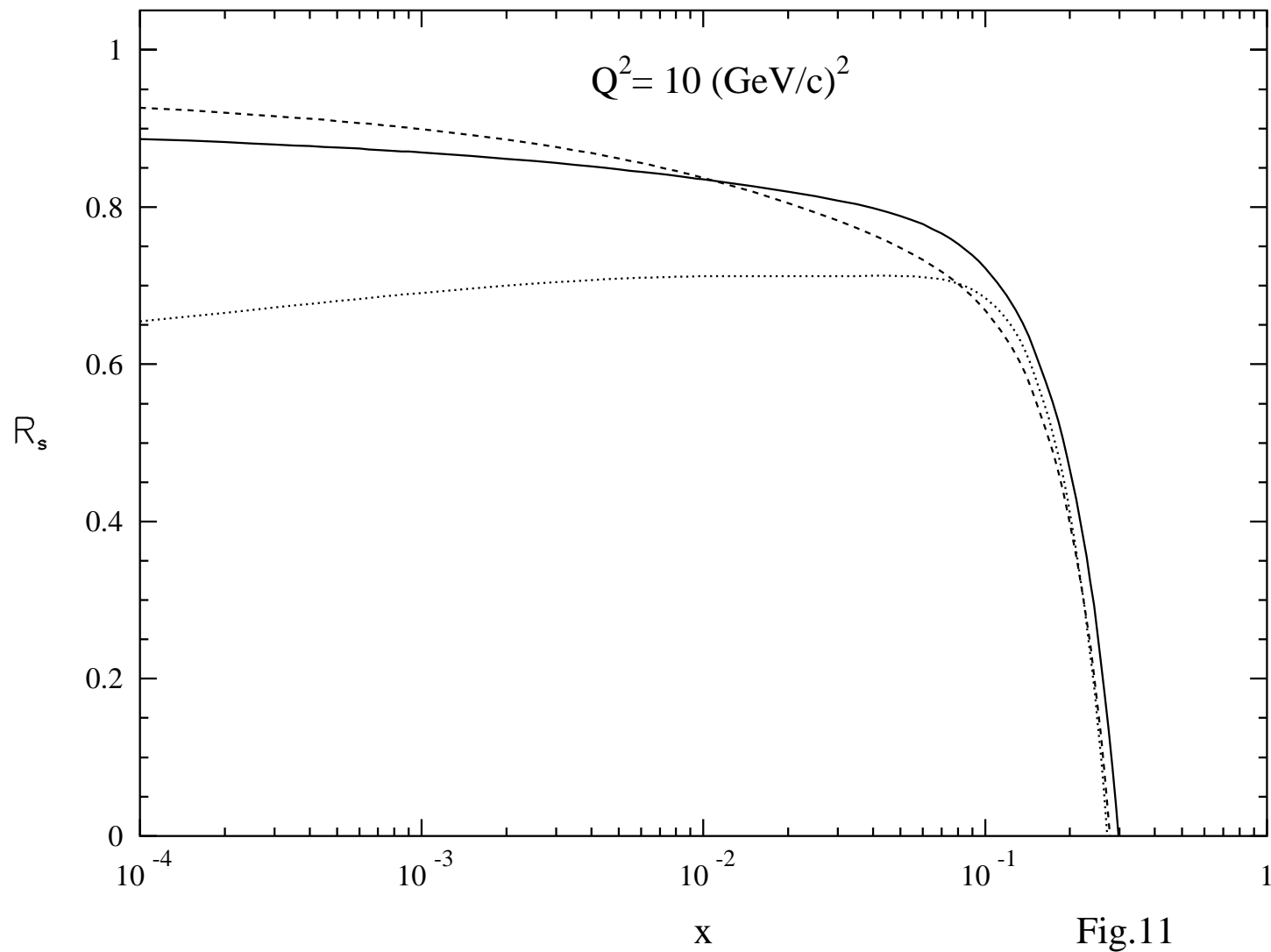


Fig.9





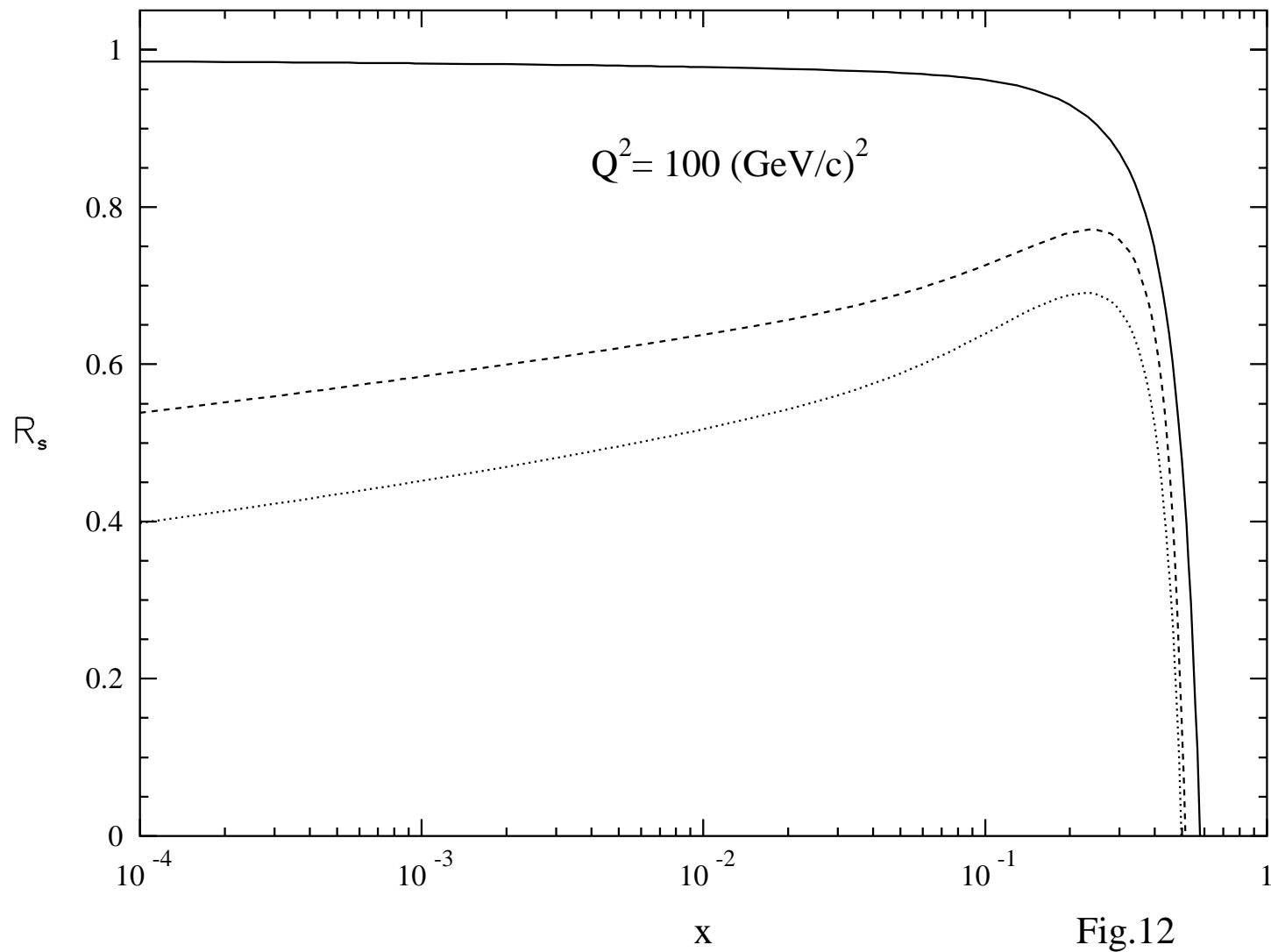


Fig.12

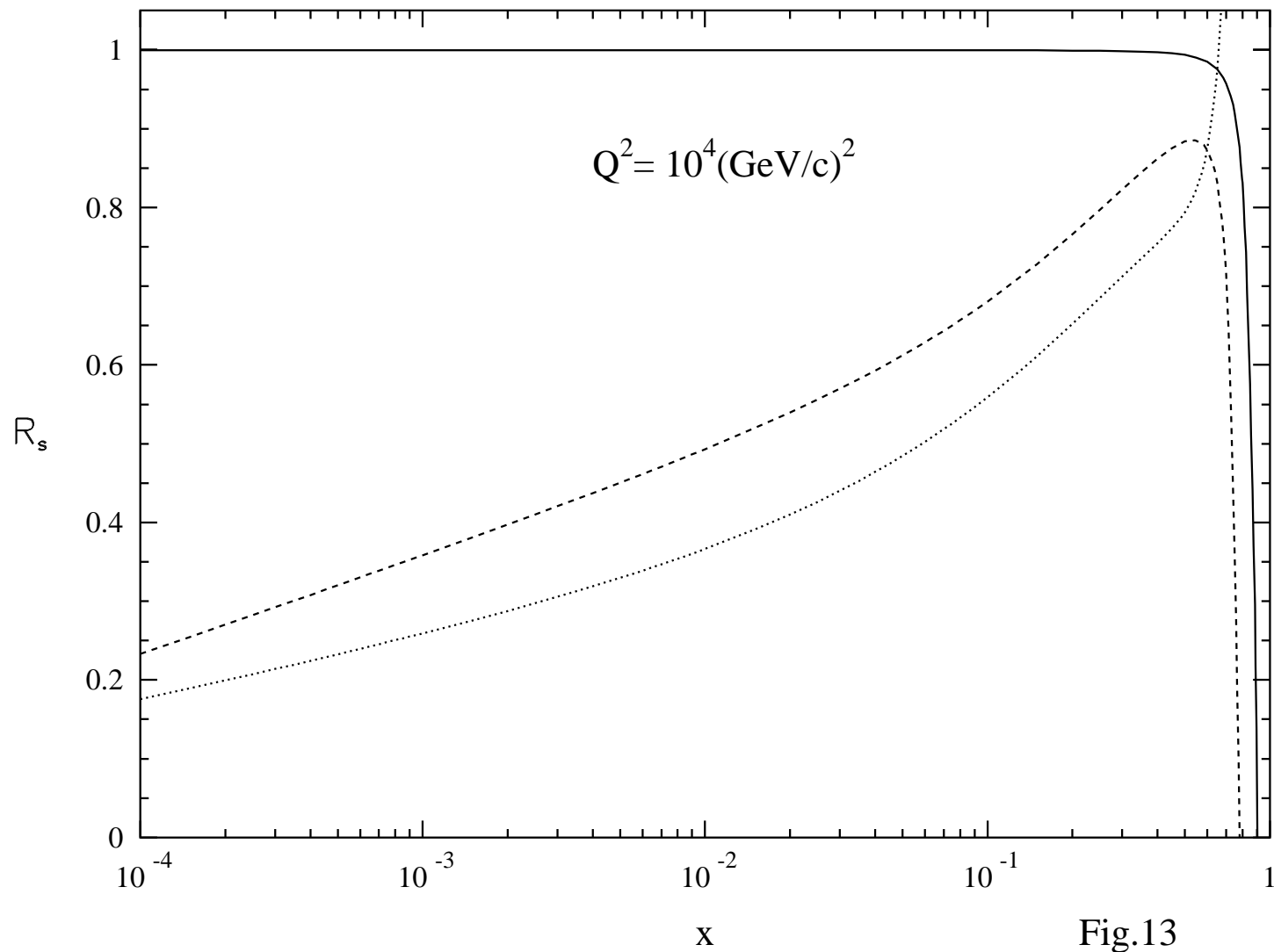
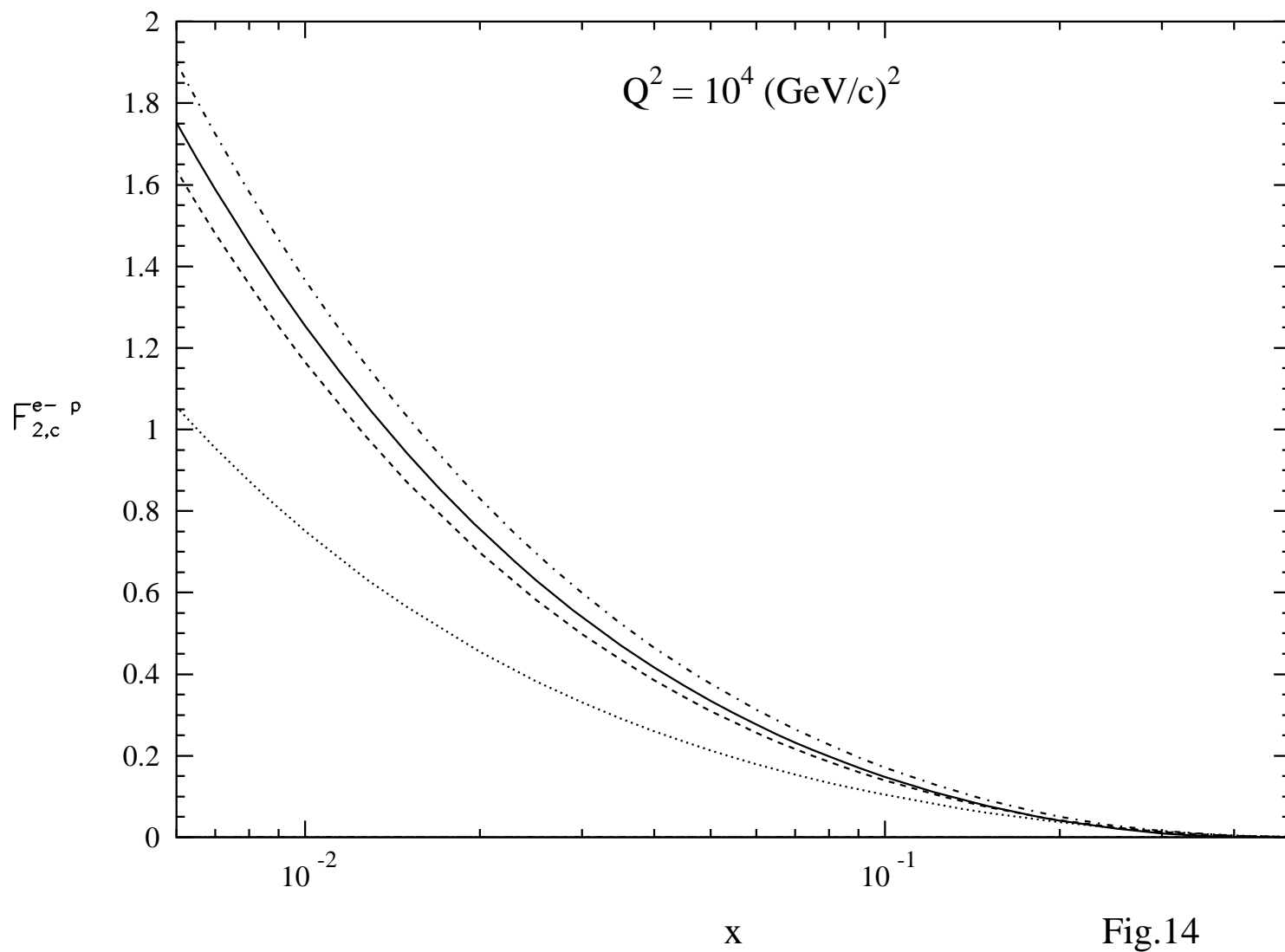
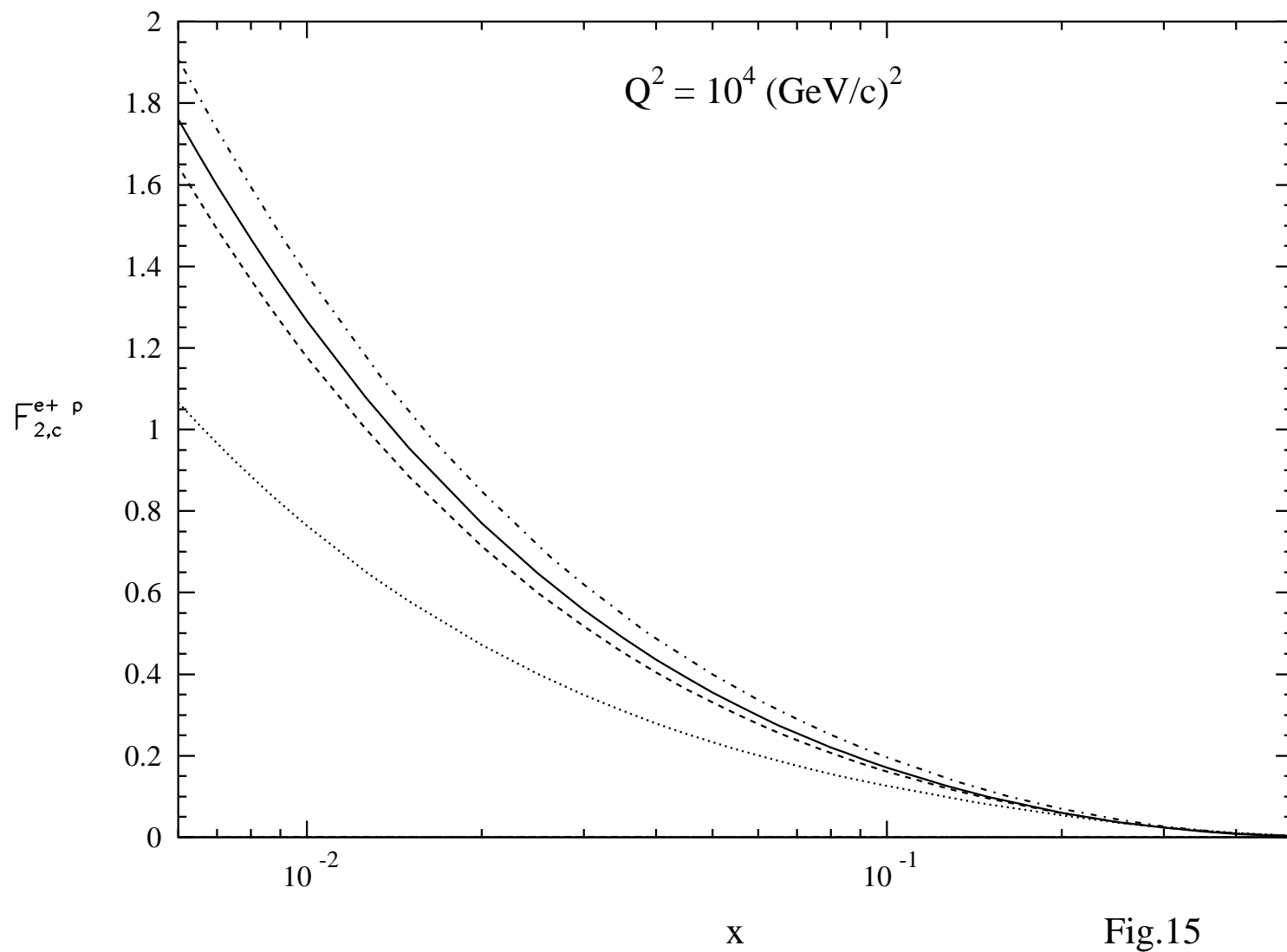


Fig.13





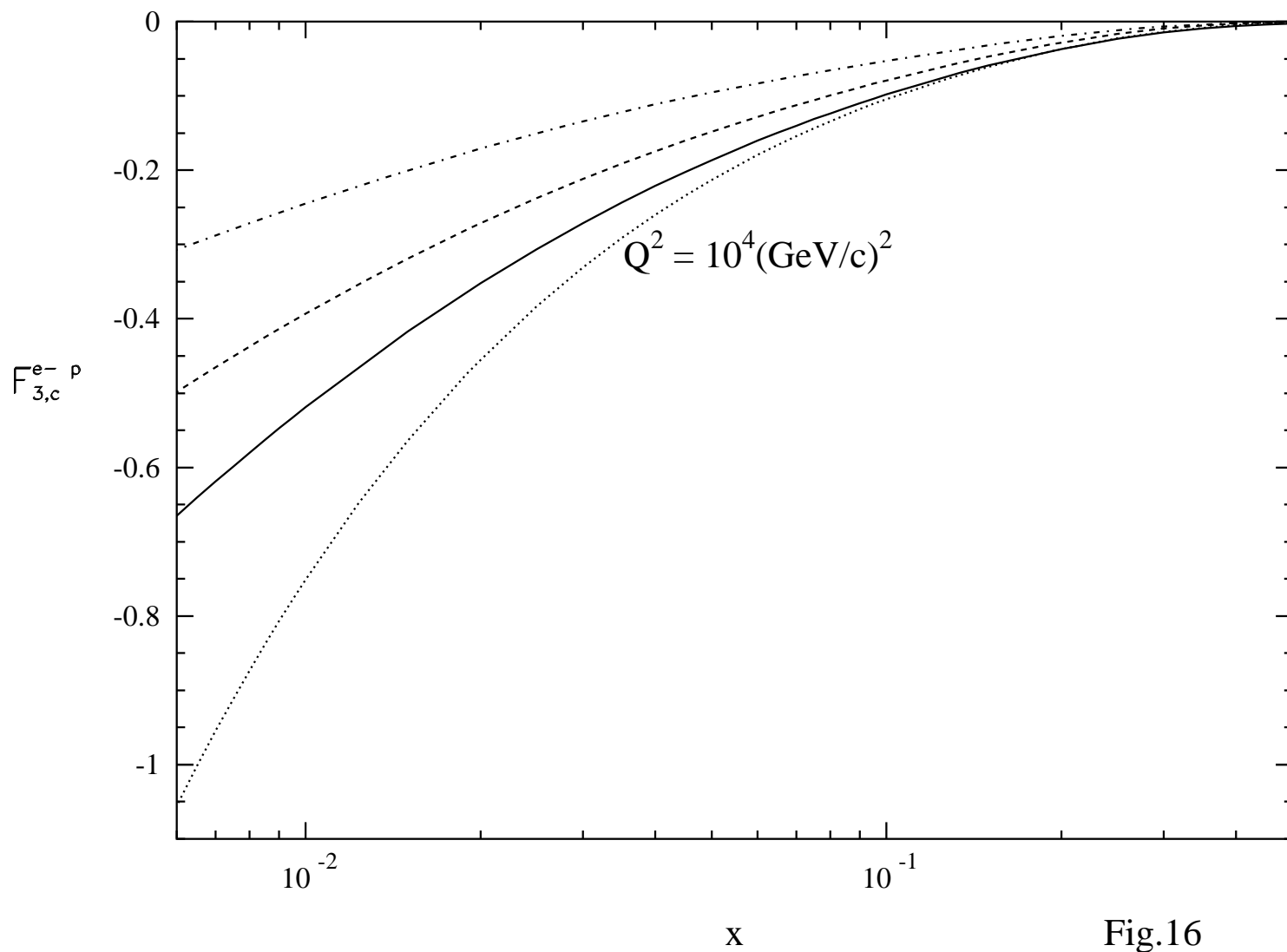


Fig.16

